Mafalda de Almeida Duarte Pina

Bachelor in Micro and Nanotechnologies Engineering

Solution Based Synthesis of doped ZnO Nanowires with Rare Earth Elements for Optoelectronic Applications

Dissertation submitted in partial fulfilment
of the requirements for the degree of

Master of Science in
Micro and Nanotechnologies Engineering

Advisor: Ana Cláudia Madeira Botas Gomes Pimentel, Researcher,
Faculty of Sciences and Technology,
NOVA University of Lisbon
Co-advisor: Joana Maria Dória Vaz Pinto Morais Sarmento,
Assistant Professor,
Faculty of Sciences and Technology,
NOVA University of Lisbon

Examination Committee:

Chairperson:	Hugo Manuel Brito Águas
Raporteurs:	Asal Kiazadeh
Vogal:	Joana Maria Dória Vaz Pinto Morais Sarmento

FACULDADE DE CIÊNCIAS E TECNOLOGIA
UNIVERSIDADE NOVA DE LISBOA

October 2019

Solution Based Synthesis of doped ZnO Nanowires with Rare Earth Elements for Optoelectronic Applications

And now for something completely different

— Monty Python

Acknowledgements

First of all I'd like to thank my supervisors for all the guidance, help and support given during the past few months. I feel really fortunate to have had the opportunity to work with such dedicated people.

I also want to acknowledge the great work done on this department (DCM) and the growth and visibility given to the nanotechnology course. To all professors et al. that contributed to my education for the past 5 years, thank you. A special thanks to CENIMAT and CEMOP (and everyone working on these institutions; everybody's always ready to help a fellow colleague).

To my family and specially my parents I thank my education and this course (even though it is a nano course, the knowledge I gained hopefully is not that small).

And I shall not forget my friends: the ones that accompanied me during this thesis, the ones that were with me through the past 5 years in FCT and all the ones that I had the pleasure to meet throughout my life. Thank you all for all the good, the not so good and the just normal moments.

Obrigada.

Abstract

Semiconductor nanostructures, and in particular ZnO nanowires (NWs), have been intensively studied due to their unique properties that allow its implementation in optoelectronic devices such as UV sensors and 1D TFTs. The doping of these NWs with rare earth elements allows to tune its conductivity and optical properties.

The present work reports the synthesis and characterization of undoped and europium doped ZnO NWs, produced through solvothermal methods assisted by microwave irradiation (MW) and conventional oven heating (CO). Different doping concentration levels were this way studied.

Both synthesis methods were successful in the production of ZnO nanostructures as confirmed by SEM and XRD, and the doping of Eu lead to the formation of $Eu(OH)_3$ nanostructures attached to the ZnO NWs. The MW synthesis lead to the formation of aggregated NWs forming nanoflowers while in the CO route the aggregation was less evident, with more isolated structures, both with average lengths of 6 μm and a very broad size distribution. Optical characterization allowed to extract the band gap (Eg≈3.2 eV). Electrical characterization was conducted on single ZnO NWs, with different alignment methodologies and in NWs with different post-annealing treatments. An optimization of the alignment strategy to add contacts to isolated NWs using conventional photolithography was achieved. In each substrate 6 individual NWs were aligned. After processing, the yield of working devices was still low as concluded from the electrical characterization where it was possible to extract a resistivity value in just 5 of the measured NWs and no trend for the resistivity values was observed. The use of a passivation layer (Parylene-C) on top of the NWs allowed to improve the stability and adhesion of the NW to the substrate.

These nanostructures were tested as UV sensors showing a responsivity of 1.5 mA/W, 1.7 mA/W and 53 μA/W for ZnO NWs without annealing, annealing at 300°C and 700°C.

Keywords: Conventional oven, Europium, Microwave, Nanowire, Solvothermal, UV sensors, Zinc Oxide

Resumo

As nanoestruturas semicondutoras, em particular nanofios de ZnO, têm sido intensivamente estudadas devido às suas propriedades únicas que permitem a sua implementação em dispositivos optoelectrónicos, tais como, sensores UV e TFTs 1D. Dopar estes NWs com terras raras permite ajustar as suas conductividade e propriedades ópticas.

O presente trabalho documenta a síntese e caracterização de nanofios de ZnO não dopados e dopados com európio, produzidos por métodos solvotermais e assistidos por radiação microondas ou aquecimento por forno convencional. Foram por conseguinte estudadas diferentes concentrações de dopante usando ambas as técnicas de síntese.

Ambos os métodos de síntese produziram com sucesso nanoestruturas de ZnO, como é verificado por SEM e DRX. A dopagem com Eu levou à formação de nanoestruturas de Eu(OH)3 agarradas à superfície dos NWs de ZnO. A síntese de MW deu origem à agregação de NWs formando nanoflores, enquanto na síntese de CO a agregação foi menos evidente, havendo mais estruturas isoladas; ambas com comprimento médio de 6 µm e uma grande distribuição de tamanhos. A caracterização óptica permitiu extrair o band gap (Eg≈3.2 eV). Caracterização eléctrica foi feita em nanofios individuais de ZnO, usando metodologias de alinhamento diferentes e NWs com diferentes tratamentos de pós-recozimento. A estratégia de alinhamento para depositar contactos num NW isolado por fotolitografia convencional foi optimizada. Em cada substrato foram alinhados 6 NWs. Depois da produção, o yield de dispositivos operacionais é bastante baixo como se verifica pela caracterização eléctrica onde só foi possível extrair a resistividade em 5 dos NWs e nenhuma tendência foi encontrada. O uso de uma camada de passivação (Parileno-C) por cima dos NWs permitiu aumentar a estabilidade e adesão dos NWs ao substrato.

Estas nanoestruturas foram testadas como sensores UV, apresentando uma responsividade de 1.5 mA/W, 1.7 mA/W e 53 µA/W para ZnO sem tratamento de temperatura, pós recozimentos a 300°C e 700°C, respectivamente.

Palavras-chave: Forno convencional, Európio, Microondas, Nanofio, Solvotermal, Sensores UV, Óxido de Zinco

Contents

List of Figures

List of Tables

Symbols

mol%	Percentage by mol
E_g	Optical Band Gap
α	Linear Absorption Coefficient
h	Planck Constant
λ	Wavelength
ν	Frequency of Vibration
A	Proportionality Constant
m	Value of the Optical Band Gap Transition
τ	Size of the Crystallite
K	Scherrer Constant
β	Full Width at Half Maximum of the Diffraction Peak
θ	Bragg Angle of the Diffraction Peak
Resp	Responsivity
R	Resistance
V	Voltage
I	Current

Acronyms

AFM	Atomic Force Microscopy
SKPFM	Scanning Kelvin Probe Force Microscopy
CO	Conventional Oven
IPA	Isopropanol
MW	Microwave
NIR	Near Infrared Radiation
NW	Nanowire
RT	Room Temperature
SEM	Scanning Electron Microscopy
UV	Ultraviolet
VIS	Visible
XRD	X-Ray Diffraction

Objectives

This work intends the characterization of ZnO nanowires produced through solvothermal methods assisted by microwave and conventional oven for application in optoelectronic devices. Morphology, structure and optical properties were studied through the analyses of SEM images, XRD diffractograms, UV-Vis spectra, and AFM.

The main objective is the electrical characterization of the single NWs produced, through the analysis of IV curves obtained in the dark and with UV light and the influence of the annealing temperature on the observed properties. With this study, it is intended to perform the optimization of synthesis and device production protocols that will allow the implementation of these NWs in future optoelectronic devices.

As a complementary objective the synthesis of europium doped ZnO nanostructures are also tested to allow the comparison between the production routes (MW and CO) and the dopant concentration (that varies between 1 and 5 mol%). The characterization techniques chosen to characterize the doped ZnO NWs were: morphological (SEM), structural (XRD) and optical (UV-Vis Spectroscopy and Raman).

Motivation

Nowadays nanotechnology has a great importance in everyday life. It is a field in constant growth where better and faster devices are expected every year. Thus, it is important the study of the nanoworld. In particular, the implementation of devices using nanostructures such as nanowires, nanorods, nanoparticles, allows to tune different properties on the materials while leading to miniaturization.

Semiconductors have an important role in electronics, making their study in new materials and new production methods to be very challenging. ZnO nanostructures are promising since the synthesis is green and relatively cheap and it can be applicable to bio-sensors, cosmetics, storage, optoelectronic devices (UV sensors, solar cells,…).

The study of ZnO nanostructures contributes to the growth and the technology development. Many challenges arise from using nanostructures, such as dispersing them in a substrate in a controlled way, alignment of the nanostructures and even their characterization. Furthermore, these nanostructures can be doped and when doping ZnO with rare earth elements the optical and electrical properties can be tuned to make it more suitable for application in optoelectronic devices.

Thus, it is necessary to study the ZnO NWs (morphological, structurally, electrically and optically) and only then an implementation of the NWs in a device can be done properly. Methodologies to align electrical contacts on randomly dispersed NWs in order to fabricate optoelectronic devices are also crucial.

Chapter 1

1. Introduction

1.1. **1D nanostructures**

Nanotechnology is considered an emerging and dynamic field that has gained attention in the last decades due to the wide range of fields where it can be applied (medicine, biology, microelectronics,…). Nanoscience studies the properties of materials at atomic and molecular scales and nanotechnology is related to structures, devices, and systems with at least one dimension below 100 nm. At such a small scale the properties of matter (optical, electrical and structural) are different from the bulk ones [1]. Regarding the dimension of the nanostructures these can be divided into four groups: 0D, 1D, 2D, and 3D. One dimension nanostructures are structures that have only one dimension above the nanoscale range (nanowires, nanorods, nanobelts and nanotubes) [2] [3].

Semiconductor nanowires are very interesting among the one-dimensional nanostructures and have been extensively studied due to their unique electronic, optical, thermal, mechanical and magnetic properties [4]. Metal oxides are ionic compounds composed by positive metallic and negative oxygen ions, and can exhibit metallic, semiconductor or insulator characteristics. Metal oxide proprieties can be engineered by modifying their size, structure, composition and by doping. Over the years these materials have been used in electronic devices with an increasing interest for the integration in sensors due to their exceptional intrinsic properties associated to their high surface-to-volume ratios, high catalytic efficiency, strong adsorption ability, and electron and phonon confinements [1] [5].

On this work the focus are the synthesis and characterization of ZnO 1D nanostructures.

1.2. **ZnO NW synthesis and properties**

ZnO (zinc oxide) is a low-cost n-type semiconductor with wurtzite structure and a wide direct bandgap (3.37 eV), a large free exciton binding energy at room temperature (60 meV), biocompatibility and ease of fabrication. This makes ZnO an efficient semiconductor at room temperature that has applications in thin films and single-crystal transistors, UV detectors, LEDs, phosphorescent glasses, piezoelectric devices, dye solar cells, photocatalytic agent, anti-bacterial and anti-fungal agents, etc [6].

In the literature, several methods to produce ZnO nanostructures were studied, such as, chemical vapour deposition, electrodeposition, electrospinning, precipitation, laser assisted flow deposition and hydrothermal methods. Nowadays we search for reliable and low-cost synthesis for

the development of nanomaterials. With that said, solution based synthesis reveals to be a promising path, since it can be considered a low-cost, scalable and easy to handle technique [7]. Most of the solution phase reaction occurs under mild conditions with a relatively low temperature. Precipitation [8][9], microemulsions [10], hydrothermal/solvothermal, sol-gel [11][12], electrochemical deposition [13] are some examples of solution based methods used to produce nanostructures [14].

In this work the synthesis processes studied were solvothermal, assisted either by microwave radiation or by conventional oven heating. The type of radiation that will promote the growth of the nanostructures will influence the final produced nanostructures. The use of microwave permits a faster and less consuming synthesis, when compared to conventional heating. This occurs because microwave radiation transfers the energy directly to the reactive species of the solution, promoting a rapid increase of temperature and originating a localized superheating of the molecules [15]. While conventional heating is characterized by energy transfer through convection, thermal conduction or radiation, microwave heating is characterized by the energy transfer between molecules (the radiation interacts directly with the solution molecules, converting the electromagnetic energy into thermal energy) [16][17].

Ultraviolet (UV) radiation is a high energy beam with photon energies varying from 3.0 to 12.4 eV (400–10 nm), which overlaps with the bandgap of zinc oxide, around 3.37 eV [7]. Therefore ZnO can be used to detect the presence of UV radiation. The mechanism that permits the detection of UV radiation is based on the adsorption and desorption of oxygen molecules on the surface of the ZnO. The oxygen molecules adsorbed to the surface of the ZnO, without any UV radiation, can capture free electrons present in the n-type semiconductor and form a low conductivity depletion layer in the near-surface region. When exposed to UV radiation (with photons with energy above the ZnO bandgap) electron-hole pairs are photogenerated, and the holes migrate to the surface along the potential slope. This potential slope is produced by band bending and discharge of negatively charged adsorbed oxygen ions through surface electron-hole recombination, leading to oxygen photo desorption. This hole trapping mechanism through oxygen adsorption and desorption enhances the high density of trap states due to the dangling bonds at the surface and thus enhances the photoresponse [18]. This working principle is represented in **Figure 1.1**.

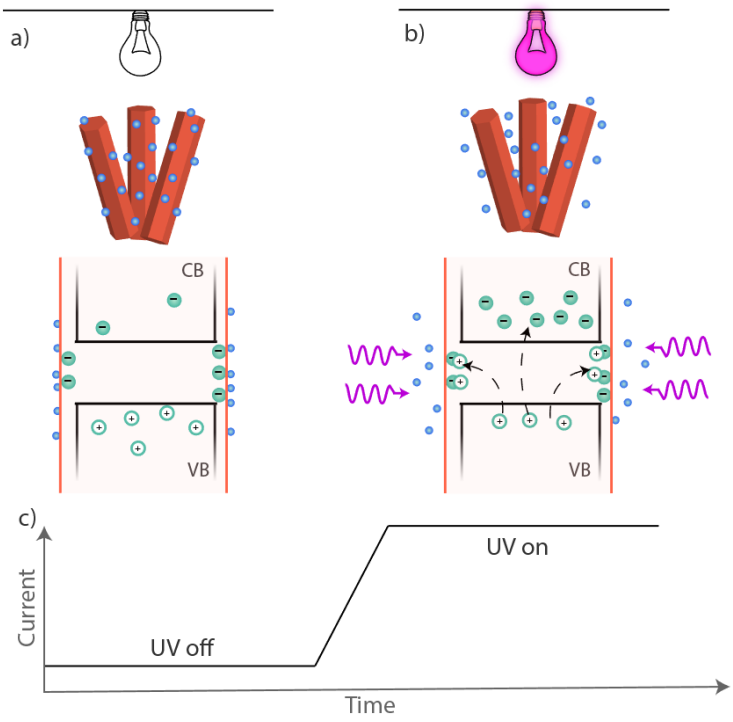

Figure 1.1 - Representation of a ZnO photodetector working principle (image adopted from [19]) a) In the dark, oxygen molecules are adsorbed on the surface of ZnO nanoparticles due to interactions with the free electrons of the semiconductor; b) Under UV irradiation, there is the creation of electron-holes pairs and the desorption of oxygen by the attraction of holes to the electrons at the ZnO's surface; c) Schematic of the photocurrent of ZnO nanoparticles in function of the UV light irradiation

1.3. **Rare earth elements**

The rare earth elements (REE) is a group of seventeen soft, silver coloured metallic elements (REEs consists of all the lanthanides plus scandium and yttrium). The name rare earth was given to this type of elements due to the difficulty chemists had in separating the elements from each other and to indicate that the REE are more stable appearing as oxides (earth) rather than metals [20]. Doping of materials with lanthanides mainly follows two different motivations: enabling new optical and magnetic properties of the modified materials [21].

Semiconductors doped with REE have been intensely studied due to their importance and potential use in optoelectronics devices such as visible (blue, green and red) and infrared luminescent devices [22]. ZnO has been extensively exploited for potential optical and photonic application with devices operating in UV region. Doping with REE can change the operating region. Most of the REE studies are focusing on Eu^{3+} doping of ZnO. For example, incorporating Eu ions can change the emission region to red [23]. However this doping process is still difficult due to the large differences in ionic radius and charge between Eu^{3+} (r = 94.7 pm, CN = 6) and Zn^{2+} (r = 60 pm, CN = 4), and the inappropriate energy level position of rare earth ion relative to the valence band and conduction band of ZnO host [23] [24].

1.4. **Optoelectronic Applications using ZnO nanostructures**

As mentioned, ZnO is widely studied due to good properties, non-toxicity and price. Research about it can be found in several areas. Direct band gap semiconductors (as ZnO) have applications in UV sensors, light emitting diodes, photodetectors, field emitters and full colour displays [25][26].

ZnO nanostructures can function as a gas sensitive material and are being integrated in gas sensors. 1D nanostructures, such as nanowire, devices are more sensitive and selective due to their high aspect ratio, resulting in a large surface area [27][28].

Since the electrical potential of ZnO nanowires changes under UV radiation, these structures are promising in UV detectors.

As for the use of single isolated micro or nanostructures progress has been made but the difficulty to handle (alignment and patterning) these nanostructures is higher. Usually high precision equipments are required [29].

Goldberg et al [29] reported the use of a single ZnO nanowire as the semiconductor in a field effect transistor successfully. It was concluded that the performance characteristics of these devices were intrinsically related with the presence and nature of adsorbed surface species.

Lin et al [30] produced and characterized two contact ZnO nanowire devices. Using field emission scanning electron microscope (FESEM) they positioned the NW on alignment marks (patterned on Si substrate) to after deposition the metallic layer through e-beam lithography. They successfully fabricated more than thirty devices and performed temperature dependent I-V curves and resistance measurements. The ZnO NWs had 40 nm of diameter and 1 μm length, the resistivity was about several mΩ.cm.

Chapter 2

2. Methods and Materials

2.1. **ZnO NWs Synthesis**

The ZnO nanostructures were synthesized via solvothermal methods, assisted by conventional heating (CO) and microwave radiation (MW). The parameters used were chosen from Coelho D. Master thesis [31] in order to insure long enough NWs to allow the use of standard photolithography procedures to align metal contacts on the NWs, and to avoid the presence of aggregated nanoflowers.

Zinc acetate dehydrate (Zn (CH3COO)2·2H2O; 98 to 101.0 %, CAS: 5970−45−6) from Alfa Aesar and sodium hydroxide (NaOH; CAS: 1310−73−2) from Eka were the precursors used. As surfactant, to stabilize and promote the growth of the nanostructures in one direction, it was used sodium lauryl sulphate (NaC12H25SO4; 95 %, CAS: 151-21-3) from Scharlau. The solvents used vary depending on the heating procedure; deionized water for conventional oven and 2-ethoxyethanol (C4H10O2; CAS: 110-80-5) from Honeywell for the microwave assisted synthesis.

A 0.45 M zinc acetate solution was prepared by dissolving the zinc acetate in deionized water and adding NaOH under constant stirring until a concentration of 8 M is reached (solution A). The surfactant solution (solution B) was prepared by dissolving the surfactant (SDS) in deionized water (with molar concentration of 1.04 mM).

For microwave synthesis it was used a CEM Mars One microwave, with capacity for twelve 50 mL Teflon vessels. Only three vessels were used where 2 mL of solution A, 5 mL of solution B and 10 mL of solvent (2-ethoxyethanol) were added into each vessel. The solutions were heated at 110°C for 30 minutes (with 7 minutes of heating ramp) and 600W of power. For the conventional oven synthesis, the same quantities were used with the only difference being the solvent (in this case it was used deionized water) and only 2 Teflon vessels (with capacity for 17 mL) were loaded into stainless steel autoclaves and then into a Heraeus furnace from Thermo Scientific. The synthesis temperature and time was 80°C and 24h.

As for both synthesis methods, after the process is complete, the vessels are let to cool down to room temperature. The white precipitate that is obtained is then washed with deionized water and isopropanol (IPA) and centrifuged at 4000 rpm for 3 min, 3 times each. The powder is then dried at room temperature for at least 72 h.

2.2. **Europium doped ZnO NWs Synthesis**

To dope the ZnO nanorods Europium nitrate ($Eu(NO_3)_3 \cdot 5H_2O$; 99.9 %, CAS: 63026-01-7) from Sigma-Aldrich with concentrations varying between 1% and 5% in mol% was used. The procedure was the same described in the previous section (2.1) with the Eu being added to solution A after the zinc acetate and before de NaOH.

2.3. **Thermal treatments**

Using a Nabertherm L030K1BN L311 B170 Muffle Furnace annealing with temperatures varying from 300°C to 700°C (with a step of 100°C) were tested on undoped ZnO NWs in both powder and on substrate dispersion. The annealing time was 2h with a heating ramp of 5 °C/min. For the NWs that were used for the single I-V tests, the annealings were performed on already dispersed NWs.

2.4. **Alignment of contacts in individual NWs**

To study the properties of single NWs, photolithography processes were carried out in order to align electrodes on both ends of a NW.

CO NWs were dispersed on top of Si/SiO_2 substrates (2.5 cm × 2.5 cm). A solution with 1 mg/mL of NWs in IPA was prepared and was submitted to an ultrasound bath for 15 minutes before the dispersion to avoid aggregation. To disperse the NWs a few drops of the solution were spin coated on the Si/SiO_2 substrate for 30 seconds at 3000 rpm and then put on a hot plate at 80 °C to evaporate the IPA. These parameters were optimized to guarantee a uniform distribution of isolated NWs on the surface. The existence of aggregates is harmful for the mask alignment process. For these reason only CO NWs were chosen [31].

Photolithography processes took place on CEMOP's cleanroom using Zuss MA45 mask aligner and using lithography masks having two identical 5 μm channel length pairs of contacts. In the same exposure 1 device having 1 NW is aligned while the other pair of contacts will be used as a blank device to have a reference of the background current.

Molibdenium was used as the metal contact and was RF sputtered using a 3" Mo target (99,99% purity) using an AJA system (rf-P = 175 W, Ar flow = 50 sccm, p-dep = 1.8 mTorr).

Two approaches were performed to align the NWs, **Figure 2.1**: **A)** deposition of the metal layer directly on top of the dispersed NWs followed by SF_6 (sulfur hexafluoride) RIE of Mo and **B)** deposition of parylene-C insulator layer on the dispersed NWs, followed by O_2 RIE (200s) of this layer, deposition of Mo and lift-off procedure of the Mo contact layer.

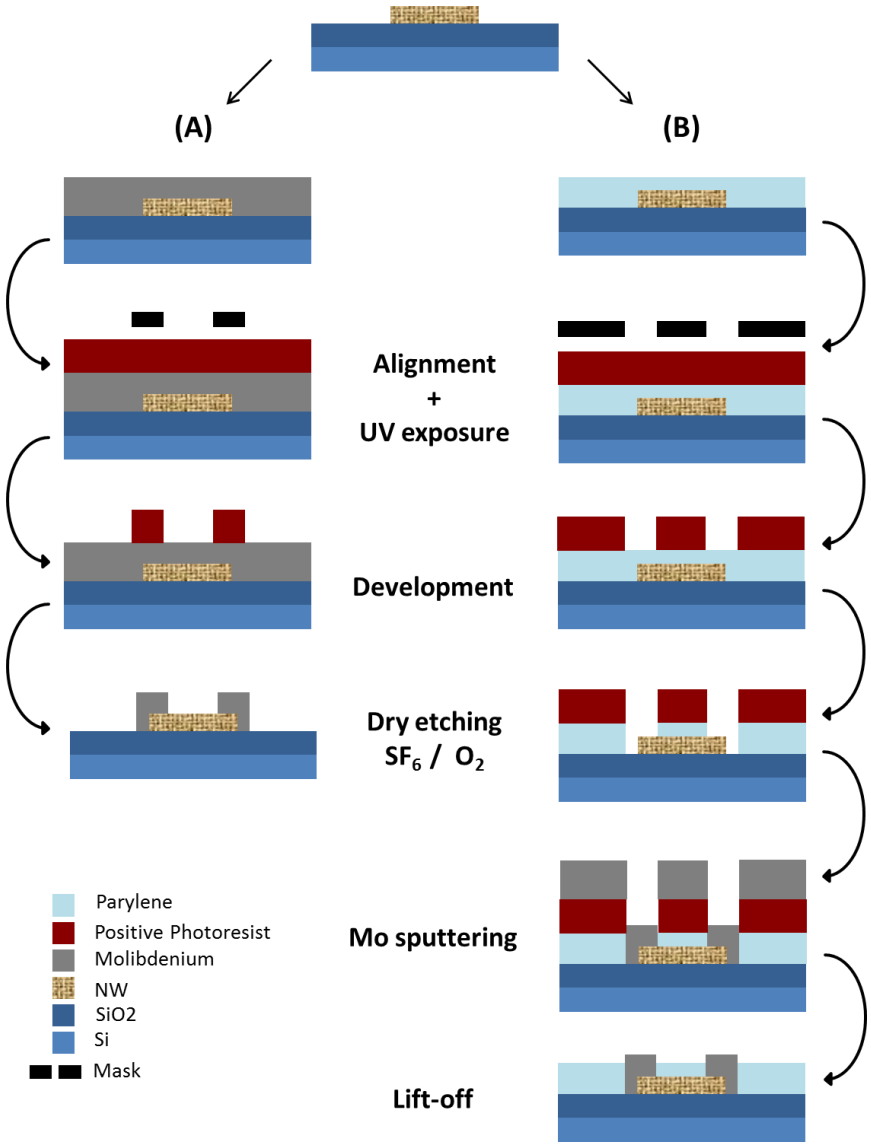

Figure 2.1 - Methods A and B for contacts deposition

For both methods was used positive photoresist (AZ ECI 3012 for method A and a thicker PR for method B - AZ 6632). The PR was spin coated at 3000 rpm for 10 s and consecutively at 4000 rpm for 20 and then put on a hot plate for 1 m 15 s at 115 °C for the soft baking. The exposure time was 6s and 10s for methods A and B. After the exposure the developer used was AZ 726 MIF.

The parylene-C deposition was performed on PDS (Parylene Deposition System) 2010 LABCOATERTM 2 by Specialty Coating Systems. The deposition occurs in three stages: firstly vaporization, where the dimer reaches the vapour state around 90 °C (to control the vaporized gas, the vaporization chamber can reach up to 175 °C); secondly pyrolysis, where the parylene gas is decomposed in monomers at 690 °C; and lastly the deposition occurs at room temperature and pressure under 16 mBar (the monomers move into the chamber and polymerize onto the substrate and a thin polymeric layer is formed).

2.5. **Interdigital contacts for UV sensors**

Interdigital contacts were used as a simpler way to test the response of the ZnO nanowires as a UV sensor. The interdigitals used were made in molybdenum with a space between lines of 30 μm. For the deposition of the nanowires onto the interdigitals it was used a dispersion of MW NWs in IPA with a concentration of 1 mg/mL. To control the area, so this is the same from sample to sample, a physical barrier of PDMS with a circular hole (0.3 mm of diameter) was placed upon the substrate. Then, using a micropipette, 1 μL of the desired dispersion was drop casted into the PDMS reservoir and put on a plate at 80 °C to evaporate the IPA.

2.6. **Characterization techniques**

The morphology of the synthesized nanostructures was analysed through SEM images. A Hitachi TM 3030Plus Tabletop and a SEM using a Carl Zeiss AURIGA CrossBeam Workstation instrument equipped with an Oxford X-ray Energy Dispersive Spectrometer were used. The crystallinity of the ZnO nanostructures was determined using a PANalytical's X'Pert PRO MPD X-ray diffractometer, with a CuKα radiation source (wavelength 1.540598 Å). Optical characterization was performed using a Spectrometer UV-Vis-NIR from Perkin Elmer Lambda 950 to obtain a spectrum from 200 nm to 800 nm to posteriorly calculate the bandgap of the nanowires. Raman spectroscopy measurements were obtained in a Raman Microscope – Renishaw Qontor. The spectra have been obtained from 60 to 2000 cm^{-1}.

For the electric characterization, a semiconductor parameter analyser (Agilent 4155 C) and a Microtech Probe station was used. The devices were irradiated with UV light using an optical fibre coupled with a high power LED (λ=365 nm). For both IV curves and UV cycles, the setup was always the same for both devices tested (interdigital contacts and individual NWs with contacts).

The Asylum MFP3D AFM (Atomic Force Microscopy) from Oxford Instruments was used to study the morphology of NWs dispersed on a gold substrate, and SKPFM
(Scanning Kelvin Probe Force Microscopy) was also performed.

Chapter 3

3. Results and Discussion

3.1. **Undoped ZnO NWs**

In this chapter, the produced ZnO nanostructures are characterized and both routes of synthesis are compared. The influence of annealing temperature on the morphological structural and optical properties is also presented.

3.1.1. Synthesis characterization (morphological, structural and optical)

Different samples were reproduced during this work, concerning the synthesis of undoped nanowires using both solvothermal routes, assisted by microwave radiation (MW) and by conventional oven (CO). The starting point of the synthesis were the optimized conditions found by a previous work [31], where different solvents and different processing temperatures are compared, in order to achieve longer than 5 μm ZnO NWs. As such, both synthesis, using water and ethanol as solvents for both MW and CO routes, respectively, were reproduced and characterized.

XRD diffractograms shown on **Figure 3.1** clearly match the hexagonal wurtzite ZnO crystalline structure (ICDD 00-036-1451), and no evidence of other phases can be detected indicating that all reagents were converted to ZnO. Using Scherrer's formula, **Equation 1**, the crystallite size can be estimated taking into account the position and width of the more intense diffraction peaks of ZnO structure.

$$\tau = \frac{K\lambda}{\beta cos\theta} \quad \textbf{(1)}$$

where τ is the size of crystallite, K is the Scherrer constant, λ is the wavelength of the incident X-rays, β is the full width at half maximum of the diffraction peak and θ is the Bragg angle of the diffraction peak (in radians) [32].

Both routes were successful in the production of ZnO and from the XRD data few differences were detected.

When comparing the crystallite size obtained through Scherer's equation using the 3 more prominent peaks of ZnO structure (100), (101) and (002) and averaging the results, the CO ZnO nanostructures showed smaller crystallite size (τ = 57.83 μm), than the MW route (τ = 74.48 nm).

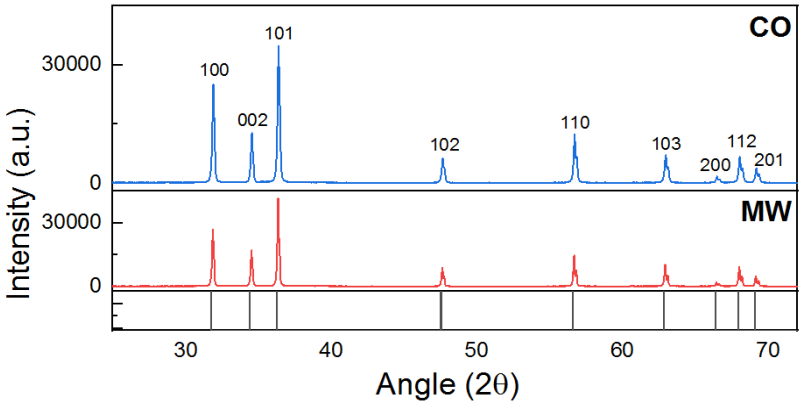

Figure 3.1 - XRD diffractograms of the MW and CO nanostrcutures and the reference used for ZnO (ICDD 00-036-1451)

In order to analyse the produced nanostructures, their shape, morphology and aggregation, SEM was used. Through SEM images, **Figure 3.2**, it is clear that the CO synthesis produced more uniform and isolated NWs with less aggregation while MW lead to more aggregation of the nanostructures and the formation of nanoflowers, which is corroborated by the literature [26][33].

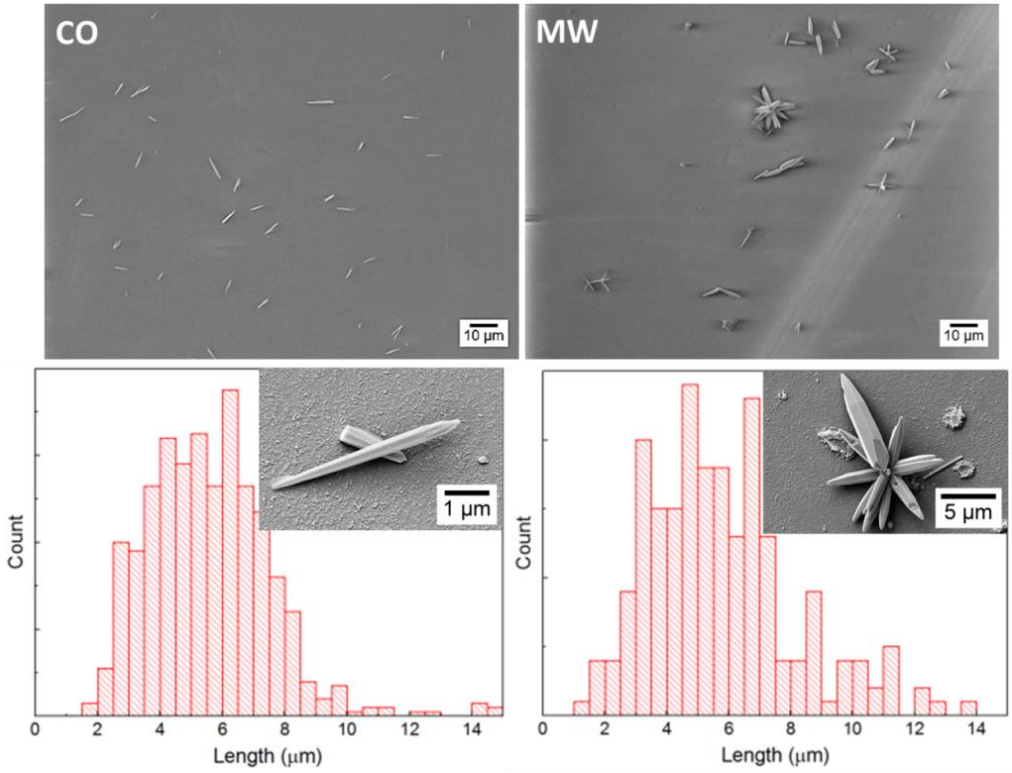

Figure 3.2 – SEM images of the nanostructures produced through CO (on the left) and MW (on the right) and length distribution

Recurring to ImageJ software the NWs dispersed on a substrate were measured – these measures took only into account the isolated NWs (the agglomerates and nanoflowers were not accounted for size estimation). The MW synthesis lead to the formation of longer NWs (6 µm) while the CO NWs lead to the formation of NWs with a mean length of 4.4 µm. As can be seen on

the histograms there's a broad distribution of length sizes with a considerable variation from the shorter to the longer NWs measures – the error associated with the mean length is high.

The analyses from SEM images and XRD peaks allowed to conclude that both synthesis lead to the formation of ZnO NWs with average lengths around 6 ± 2 μm and having a very broad size distribution.

Annealing was performed on the synthesised powders. The main goal was to test how this themal treatmemt would affect the morphology and structure of the NWs, and consequently the electrical and optical properties of the NWs. Furthermore, since one of the objectives was to dope the NWs, annealing treatments are usually required to facilitate the lattice incorporation of the dopant [34][35].

The characterization of the NWs subjected to thermal treatments showed that the nanostructures tend to aggregate with temperature resulting in bigger agglomerates, leaving the smaller NWs isolated. This means that the annealed NWs measured have a smaller mean length than the NWs that did not go through an annealing process since the NWs that were measured were only the isolated ones.

To prevent aggregation for some characterizations techniques, annealing treatments were performed on nanostructures already dispersed on a Si substrate. These substrates were the ones used in the electrical characterization as it will be explained further on the document.

Optical spectra were obtained for the different powders and recurring to Tauc plots [7][36] the band gap was calculated (Apendix A – Tauc Plots (bandgap calculation)). Both synthesis routes lead to Eg close to 3.15 eV as reported in the literature [37][38].

On **Table 3.1** it is summarised the length, crystallite size and optical band gap for the undoped ZnO NWs for different annealing temperatures.

Table 3.1 - Length, crystallite size and optical bandgap for the undoped ZnO powders with and without annealing treatment

	CO			**MW**		
	Length [μm] ± 2 μm	**Crystallite size [nm]**	**Eg [eV]**	**Length [μm] ± 2 μm**	**Crystallite size [nm]**	**Eg [eV]**
RT	4.4	57.8	3.140	5.7	74.5	3.060
300 °C	4.2	57.4	3.195	4.7	78.2	3.161
400 °C	4.1	64.7	3.190	4.4	78.4	3.138
500 °C	3.9	79.3	3.164	4.8	94.1	3.132
600 °C	3.8	78.4	3.184	4.8	80.3	3.162
700 °C	3.5	75.1	3.187	5.6	74.0	3.161

This characterization allowed to conclude that the synthesis were successful in producing ZnO NWs with dimensions suitable to be aligned by conventional photolithography and used in optoelectronic devices. The MW synthesis lead to more aggregated NWs, in flowerlike structures, while CO lead to less aggregated NWs, more suitable to be incorporated in a 1D optoelectronic device.

3.1.2. Electrical characterization of ZnO nanowires

After the synthesis and structural characterization of ZnO NWs, a focus was given to the electrical characterization. For such, electrical contacts are required to collect current/voltage characteristics of the nanostructures. Since ZnO is a well known UV sensitive material, the characterization followed two types of devices: i) UV sensor response using randomly dispersed ZnO NWs on interdigital electrodes and ii) individual ZnO NW characterization through alignment of electrical contacts through photolithographic processes.

3.1.2.1. UV sensors

In order to test the response of the NWs to UV radiation, interdigital electrodes were produced having 30 μm gap separations. The NWs were used in a concentrated solution and drop casted on top of the electrodes, using a circular PDMS reservoir. They were mounted on a microprobe station and irradiated using a UV LED of 365 nm, mounted at 1 cm from the device, being the electrical characterization of these devices performed both in dark and under UV irradiation.

On **Figure 3.3** it is represented the response of a UV sensor produced with undoped ZnO nanostructures and an image of the corresponding device where is possible to see the nanostructures distribution. The distribution of nanostructures is not uniform throughout the sample, with a larger concentration of nanostructures along the borders. Even from sample to sample it is possible to see a great variation on the quantity and distribution of the nanostructures (**Appendix A**). This does not allow a rigorous comparison between samples since the response of the device is related to the quantity of nanostructures present. It is still possible to see that the ZnO NWs are sensible to the UV radiation: the current increases from 0.9 μA to near 5.6 μA when UV irradiation takes place, and reduces back as soon as the UV LED is off.

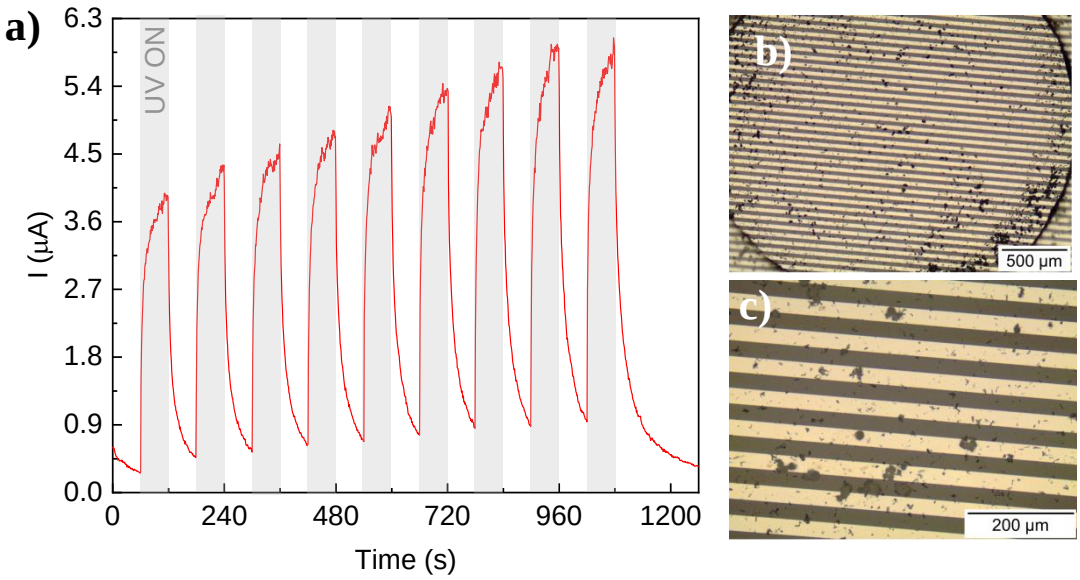

Figure 3.3 – a) UV response for undoped ZnO without any annealing treatment (V=5 V) b) and c) images of the device area with different magnifictions

However it is very difficult to study how the annealing affects the optical and electric properties through these interdigital devices. A more uniform process to deposit the NWs upon the interdigital contacts is this way required. A common approach would be to disperse the NWs in a binder to insure a deposition covering the full area of the sensor, and the production of different sensors keeping constant the concentration of dispersed NWs.

The responsivities [19][39] for the tested sensors were estimated according to **Equation 2** and are presented in **Table 3.2**:

$$Resp = \frac{I_{PH} - I_{dark}}{P_{UV}} \qquad \textbf{(2)}$$

where Resp is responsivity, I_{PH} is the current when irradiated with UV light, I_{dark} is the current in the dark and P_{UV} is the LED power. Values for the I_{dark} and the corresponding resistance value are also presented for comparison.

Table 3.2 - UV sensor parameters obtained using ZnO NWs

Undoped ZnO	$\mathbf{I_{dark}}$ **(A)**	$\mathbf{R_0}$ **(Ω)**	$\mathbf{(I-I_{dark})/\ I_{dark}}$	**Resp [mA/W]**
RT	8.97×10^{-7}	5.58×10^{6}	5.49	1.5
300 °C	8.27×10^{-7}	6.05×10^{6}	7.19	1.8
700 °C	4.53×10^{-8}	1.10×10^{8}	4	0.05

The I_{dark} current was in the same range for all measured sensors corresponding to resistance values of MΩ although a resistivity value cannot be extracted due to the non-uniform sample coverage. A gain can however be extracted indicating that these nanostructures do respond to UV light and are good candidates to the production of UV sensors.

3.1.2.2. Electrical characterization of isolated NWs

The main objective of this thesis was the production and electrical characterization of ZnO NWs. In order to be used in a device, either a uniform coverage of a surface is required or the implementation of devices using isolated NWs. This last option involves alignment procedures in order to deposit metallic contacts on both ends of the NWs, representing a huge challenge considering the broad distribution of NW sizes and tendency to aggregation of both synthesis routes.

Electric characterization was performed on the isolated RT ZnO NWs and on the annealed NWs (300, 400, 500, 600 and 700 °C) dispersed on Si substrate. This alignment was only performed on the NWs produced through CO because this route leads to fewer agglomerates and no nanoflowers when compared to the MW synthesis. The nanoflowers and bigger nanostructures (agglomerates) are harmful and undesired on photolithography processes because these structures can damage the mask.

The procedure for the NWs alignment followed two different methods (A and B) that are summarized and described in **Figure 2.1**.

During the fabrication procedure several problems may arise that will be briefly explained: i) the alignment of the NW with the contacts is limited by the optical resolution of the microscope in the mask aligner, meaning that some NWs are tilted and it is hard to confirm that the contacts will be correctly aligned in both ends; ii) The exposure is performed in contact mode, and even if the alignment was the correct one, when in contact the presence of aggregates in the vicinities may induce some shift and tilting of the mask/sample; iii) The development and PR removal is performed in liquid solution, by gently movements of the sample. In this process the NW may get louse and washed away. This is more critical for Method A than Method B where Parylene also serves as encapsulation, keeping the NW on the surface.

With the alignment Method A, 6 substrates were prepared (one for each temperature of annealing and one for RT NWs). For the alignment Method B (with passivation layer), 3 substrates were prepared (RT, 300 °C and 700 °C). On each substrate, the alignment of 6 NWs was attempted.

To analyse and characterize these NWs, SEM images and IV curves were obtained for all devices. The IV measurements were also compared with the blanks IV curves that served as reference for the background current.

For the method A only 2 devices were successful (the NW had an electrical response superior to the blanks): one NW annealed at 600 °C and another NW that suffered annealing at 700 °C. 10 of the NWs were not correctly aligned at both ends which was only confirmed afterword through SEM images. An example of the alignment difficulties is represented on **Figure 3.4** with a) the alignment failing in one of the ends of the NW and b) with more than one NW being aligned (there is more than one nanostructure in the channel).

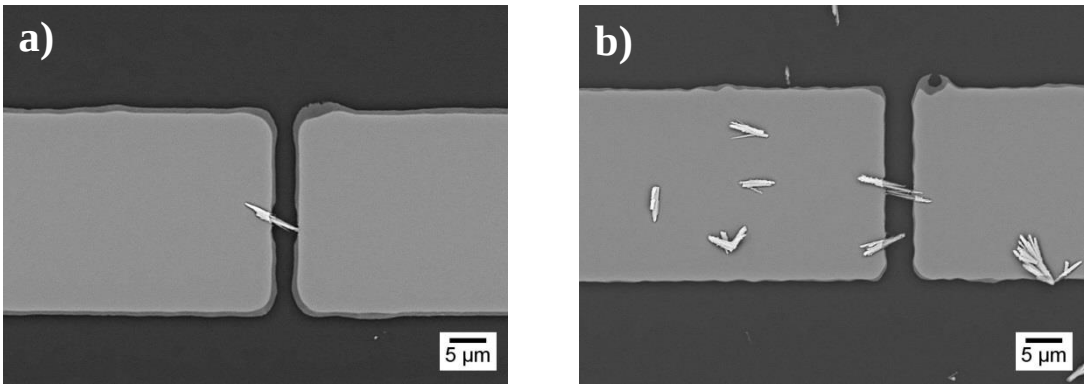

Figure 3.4 – Alignment dificulties; a) failled alignment on one end of the NW, b) aligment of more than a single NW

With method B the yield of working devices was superior with 7 NWs: three NWs without annealing (RT), two NWs annealed at 300 °C and another two NWs annealed at 700 °C. Again a relatively high number of NWs were misaligned, with results similar to the ones showed in Figure 3.5. In some NWs, although SEM images revealed nice alignments, there was no current measured; SEM also showed a non uniform Mo contact. This problem was only encountered in the method B for the annealing at 300 °C and is due to a bad revelation of the PR after the UV exposure – rests of PR were left on the electrodes area leading to holes after the liftoff, as can be seen in **Figure 3.5**. This was critical for 4 out of the 6 aligned NWs, with no current being measured (the IV obtained was very similar to the blank).

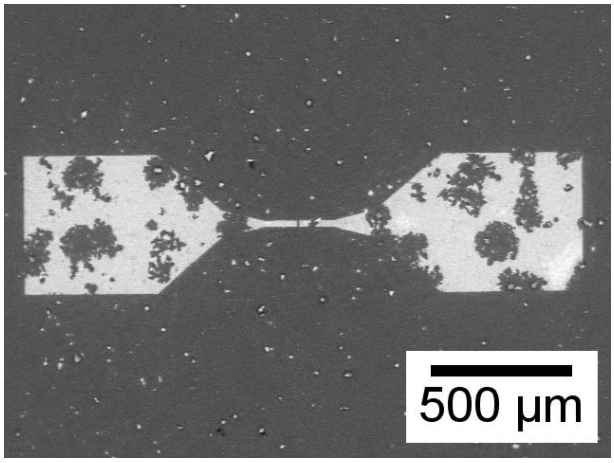

Figure 3.5 – Non uniform Mo electrical contacts

In both methods, the alignment process itself is thorough and requires patience and time. Some of the procedures failed to align a NW between the two electrodes (some NWs were only aligned on one end, others had more than one NW between the two electrodes, etc).

All the blanks measured had currents below 10^{-10} A, so this is the level of current used as reference (to consider that the response obtained is from the NW the current needs to be higher than that).

For each NW the IV curve is first compared with the blank. Checking with the SEM image of the channel this allows to conclude if the electrical response is from the NW. In **Figure 3.6** is represented the plotted curves for one NW from method A annealed at 700 °C and its blank, in logarithmic scale showing a difference of 5 orders of magnitude between the blank and the NW. The linear IV curve is plotted with the leakage current (that is on the order of pA) and with the SEM image it is confirmed that there is a well aligned NW.

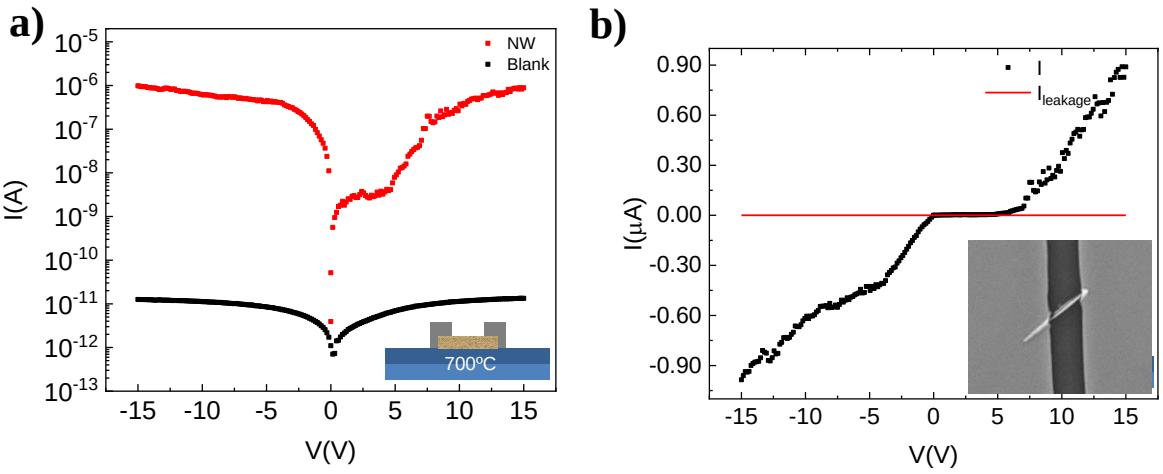

Figure 3.6 – Method A (NW annealead at 700 °C): **a)** NW and blank in logarithm scale, and **b)** linear I-V with leakege current and SEM image

For this particular case, a rectifying behaviour can be extracted from these curves, indicating two different conductive regions, possibly due to contact resistance between the Mo contact and the ZnO NW.

From the linear graph, the resistivity (ρ) of the NW can be calculated using the **Equation 3**:

$$\rho = \frac{R \times A}{L} \qquad \textbf{(3)}$$

where the resistance (R) can be extracted from the linear fit of the IV curve, the length (L) is the distance of the NW between the two electrodes and the area (A) corresponds to the NW cross section where it is assumed that the width of the NW equals the diameter of a circular cross section.

All the curves and images of the working devices can be consulted in **Appendix C** – Individual NW characterization, as well the part of the graph from where the resistance was extracted.

In **Figure 3.7** it is shown an example of a NW and blank curve obtained for method B. In this case it is a NW annealed at 300 °C. Comparing with method A, the current of NW is higher (around 2 orders of magnitude).

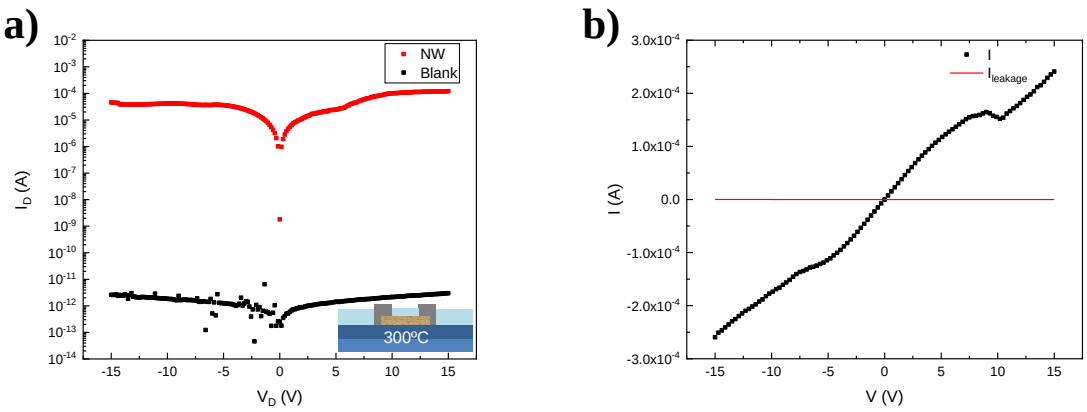

Figure 3.7 - Method B (NW annealead at 300 °C): **a)** blank and NW in logarithm scale, and **b)** linear IV curve and SEM image (right)

Table 3.3 summarizes the number of working devices and the calculated resistivities for all working devices. There is a big variation between the calculated values and this can be related to the region of the graph from where the resistance is extracted. Some of Method B devices considered were from more than one NW aligned that formed a channel between the two electrodes. These NWs are identified with a * and the SEM images can be checked on **Appendix C**.

Table 3.3 – Working devices obtained and the calculated resistivities, and yield of methods A and B

	Method A				Method B			
	#	ρ [Ω.cm]	L [µm]	Diam [µm]	#	ρ [Ω.cm]	L [µm]	Diam [µm]
RT	0	-	-	-	3	0.61 *	5.95	0.45
						0.42 *	6.30	0.40
						2.24 *	7	1
300 °C	0	-	-	-	2	42.41	5.40	0.5
						7×10^{5}	8.20	0.5
400 °C	0	-	-	-	-	-	-	-
500 °C	0	-	-	-	-	-	-	-
600 °C	1	8.21×10^{3}	5.70	0.45	-	-	-	-
700 °C	1	46.18	4.30	0.53	2	57.21	5.80	0.65
						40.08 *	5.50	0.40
Yield	**2 / 36** (5.56%)				**5 / 18** (27.78%)			

***** Alignment of more than one NW in the same channel

When comparing the numbers of working devices obtained through each method and its yields it is clear that method B is superior. The passivation layer (parylene film) increases the adhesion of the NWs to the substrate and facilitated the photolithography process. Some of method A devices broke down during the electrical characterization. With higher voltage applied the IV curve became as the blank. After the electrical measurement the channel was seen through SEM image where, in same cases, the NW had disappeared. In other cases it seems that the NW in the middle had melt or disintegrated. This only happened on method A NWs, with no case registered for method B (even with tension applied equally high).

The values obtained have a big variation and just only a few NWs were measured. In literature the values for the ZnO resistivity depend on various factors such as the synthesis method and the type of nanostructure. Calculated values for the resistivity of ZnO NWs (obtained from other methods than solvothermal), from published works obtained values in the range of few mΩ.cm [30][40] and 10^{5}-10^{6} Ω.cm [37][41].

The values calculated in this work fall between the information found in literature, where there is a broad range of values.

The number of working devices increased (comparing with the previous work) due to expertise gained during the processing. Method B revealed to be more reliable although more working

devices on the same substrate are still needed to be able to trust the resistivity values and to confirm if there is a tendency with post-annealing treatments on the NWs.

Once the ZnO is sensible to the UV radiation, IV measurements were also done with UV light irradiating the devices. The same devices presented previously in Figure 3.5 and Figure 3.6 were chosen for **Figure 3.8** where the response of the devices when irradiated with UV light is compared with the measurements in the dark and with the blank reference (for both methods). It is clear that the current increases with UV radiation on both methods.

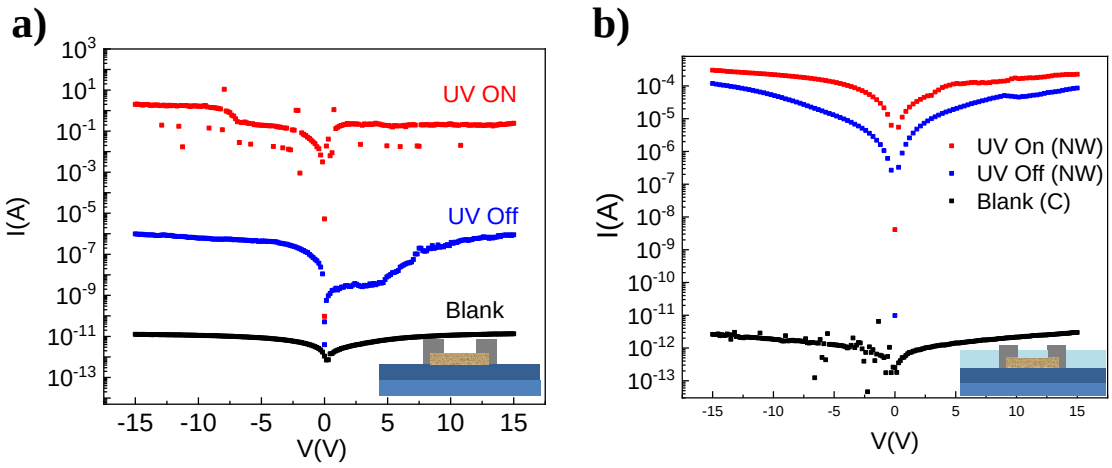

Figure 3.8 – IV curves for blank, NW in the dark and NW with UV light for method A (**a**) and method B (**b**)

When comparing the photocurrent evolution the method A device has a higher increase (from dark to the UV On measurement), becoming in the order of the Amperes, while in the method B device (the one with the parylene passivation layer) the increase does not reach one order of magnitude. This can be related with the UV sensing process that has to do with the adsorption and desorption of O_2 molecules. The parylene layer may work as a barrier not allowing these molecules to adsorb [42].

In these devices that show a response to the UV light, I-t curves can be obtained. This test was only done for two devices of method B. In **Figure 3.9** is presented the curve obtained for method B device that was annealed at 700 °C.

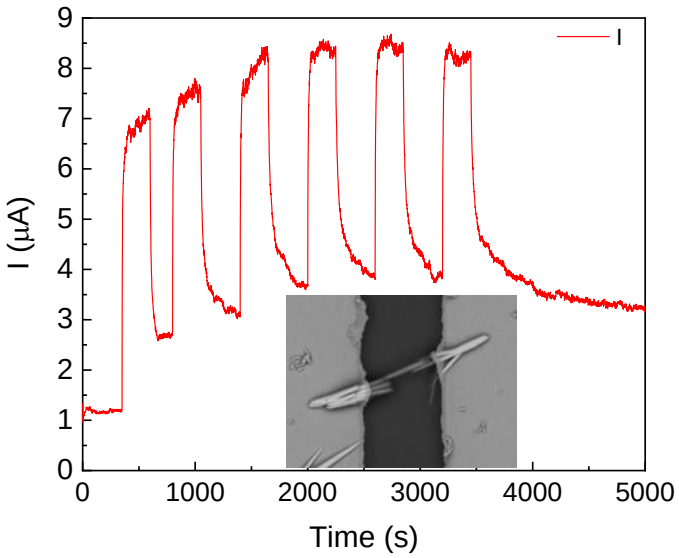

Figure 3.9 – I-t curve for a device of method B annealed at 700 °C (with an applied constant V_D of 5V)

A 6 cycle of UV on/off is performed with the duration of cycles being different: 250s on and 350s off. Devices passivated with parylene showed that the recovery to the initial I_{dark} takes even longer, seen by the increasing minimums.

The UV response was confirmed in 4 devices (one from method A and 4 from method B). The comparison between the IV in the dark and with UV light showed an increase of around of one order of magnitude for all method B devices tested. Method A has a higher increase, which indicates more sensitivity to the UV light. The UV cycles were only performed on 2 method B NWs but it would be interesting to see if the stability of a method A device is as good as method B.

3.1.2.2.1. **KPFM characterization of the NWs**

KPFM was performed on CO NWs dispersed on gold substrates. The substrate chosen was the same for samples in order to have a reference background equal in all measurements. **Figure 3.10** is an example of the data obtained for the samples: an image of the topography and a 4D image where the topography and the contact potential difference (the colour bar) can be seen.

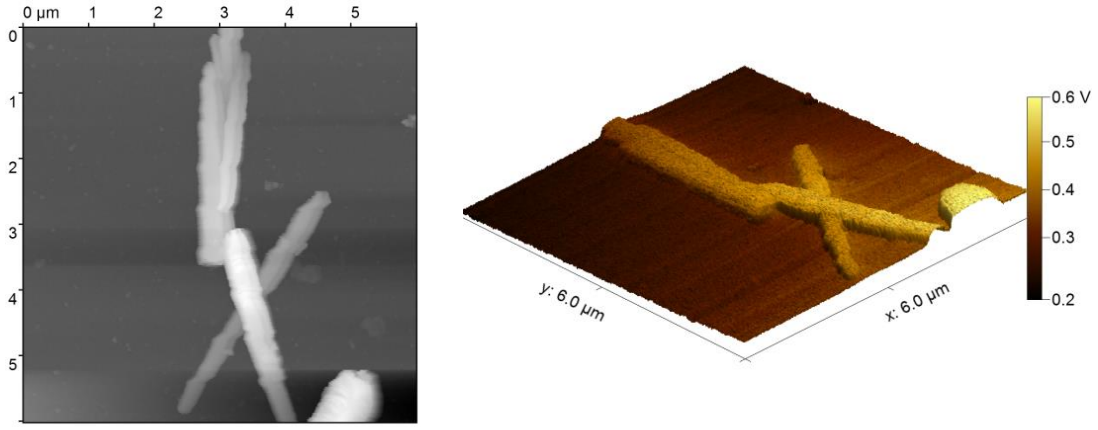

Figure 3.10 – Image of topography on the left, and 4D KPFM of ZnO NW annealed at 500 °C (surface potencial on the colour bar) on the righ

Through the data obtained and **Equation 4**, the work function of the NW [43] can be estimated:

$$V_{CPD}^{Tip} = \left(\frac{\phi_{Tip}}{-e} + V_{Ext}\right) - \left(\frac{\phi_{Sample}}{-e}\right) = V_{CPD} + V_{Ext} \qquad \textbf{(4)}$$

where V_{CPD}^{Tip} is the contact potential difference (obtained from the map), V_{ext} is the external voltage applied on the tip, the ϕ_{tip} is the work function of the tip (which in this case is platinum), the ϕ_{sample} is the work function of the sample and *e* is the elementary charge. To calculate the work function it was considered the V_{CPD} difference between the NW and the gold, since the V_{CPD} measured for the gold varies between samples. Doing this ΔV_{CPD} (variation) it is expected to minimize the error associated with the measure between samples. In **Figure 3.11** all the surface potential images obtained for the several samples are represented, with the points used to extract the V_{CPD} values indicated.

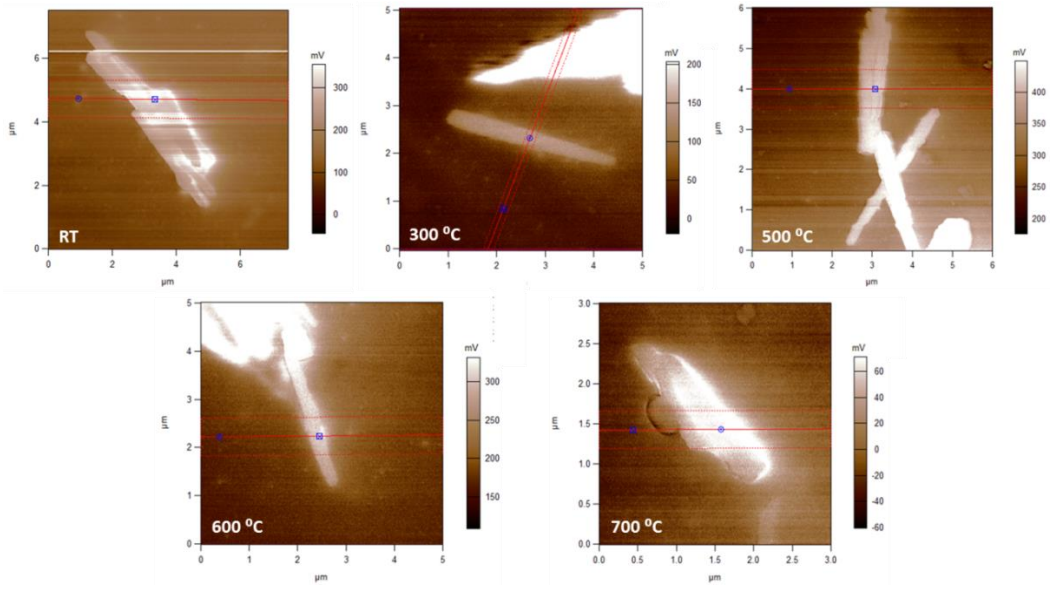

Figure 3.11 – SKPFM images for RT NW and NWs annealead at 300 °C, 500 °C, 600 °C and 700 °C

Considering the work function for gold (ϕ_{Au} = 5.47 eV), the work function for the NWs was calculated, **Table 3.4**. The values obtained are plotted, **Figure 3.12**.

Table 3.4 – Calculated workfuntion for the NW with annealing

CO [°C]	ϕ_{NW} [eV]
RT	5.66
300	5.55
500	5.64
600	5.60
700	5.57

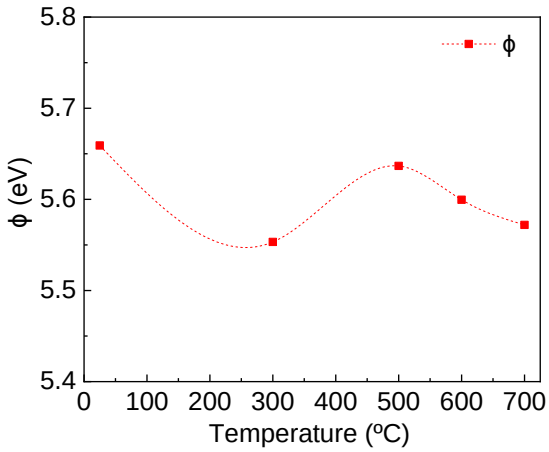

Figure 3.12 - Graphic representantion of the tendency of the workfuntions of the NWs with temperature

Comparing with the RT NW, all the NWs that were annealed have a lower work function. For the 500 °C, 600 °C and 700 °C there is a tendency with the work function decreasing with temperature. This technique cannot be considered as a true quantitative measurement due to the facts that measurements were not performed on the same day and tip wearout must be considered. Furthermore for a true quantitative analyses this measurements should be performed in vacuum.

In literature it is found that ZnO has a work function of 5.2 eV - 5.3 eV [44][45][46].

This technique seems promising in the characterization of individual NWs. Several measurements of the same NW should be done to confirm the values obtained. To extract the size of the NW this measurement is also more precise than the one based on the SEM image (in this method the error associated with the measurement is higher).

3.2. **Europium doped ZnO NWs**

As done before for the undoped ZnO, the Eu doped ZnO NWs are characterized morphologically and structurally recurring to SEM images and XRD diffractograms. Optical characterization is also performed through the calculation of the bandgap.

3.2.1. Synthesis characterization (morphological, structural and optical)

Analysing the SEM images it can be seen that both synthesis routes (CO and MW) produced NWs. The MW route lead to the formation of nanoflowers and apparently to smaller nanowires while the CO synthesis produces longer NWs. With the increase of mol% of dopant, the NWs produced are smaller and there are more agglomerates. This indicates that the synthesis parameters

need to be optimized so the aggregation is minimized and the produced NWs are longer (to be suitable for the individual electrical characterization).

In **Figure 3.13** is clear that there are some nanostructures attached to the ZnO NWs. With the increase of dopant in the synthesis, the NWs have more of those nanostructures attached which indicates that the NWs are not being doped and that the europium is forming another phase in the surface of the ZnO NWs.

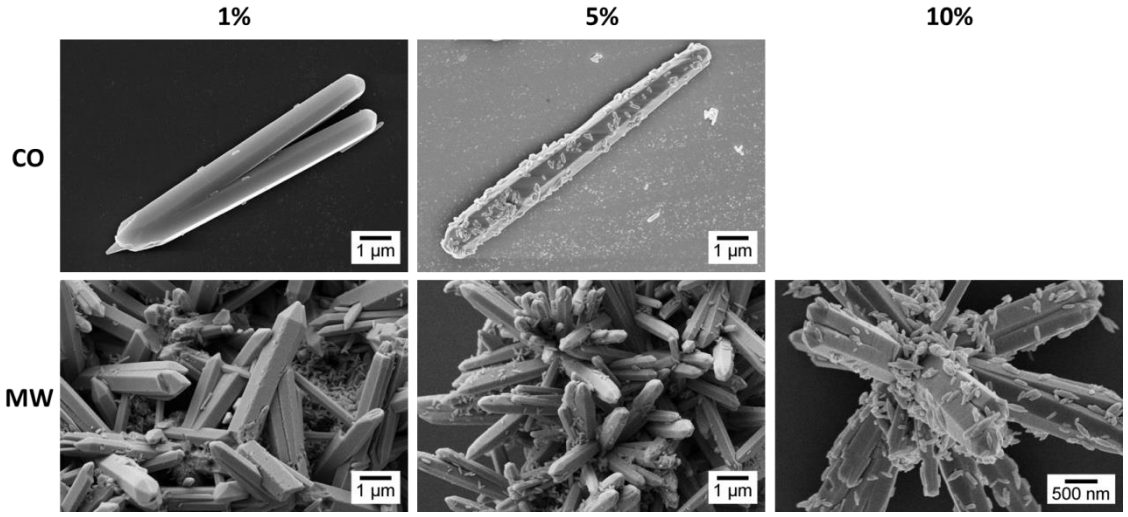

Figure 3.13 – SEM images for the Eu doped ZnO NWs for both synthesis routes (CO and MW)

For the structural characterization, XRD for the several doping concentrations (1% to 5% for CO and MW plus 10% for MW) is performed. The ZnO crystalline wurtzite structure can be identified (ICDD 00-036-1451). The crystallite sizes calculated showed that the MW NWs are more crystalline (94.5 nm) than the CO (79.9 nm), as for the undoped ZnO NWs. Two extra peaks (28.25° and 29.48°) can be identified which correspond to ($Eu(OH)_3$). The intensity of these peaks increases with mol% of dopant present in the sample, **Figure 3.14**. This indicates that the nanostructures that are forming on the surface of the NWs might be $Eu(OH)_3$ since both the quantity of nanostructures and the intensity of the peaks increase with increasing mol% dopant.

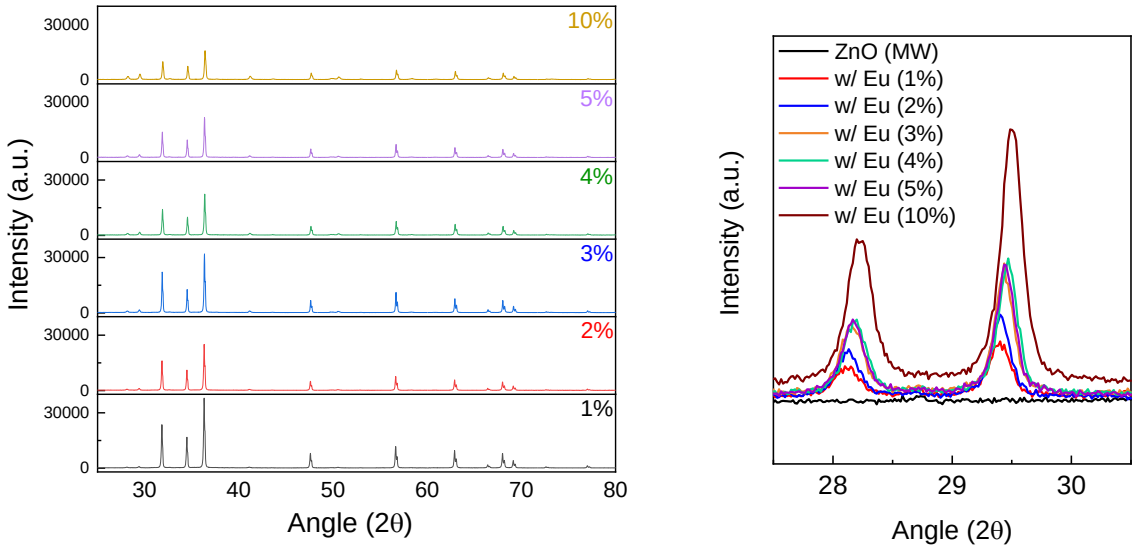

Figure 3.14 – XRD diffractograms for Eu doped ZnO (on the left) and the increase of intensity for the $Eu(OH)_3$ phase (on the right)

In-situ XRD was performed to test the behaviour of the NWs with temperature. The sample chosen was MW with 2% of Europium. It was heated to 700 °C with measurements being made every 100 °C. Analysing the diffractograms obtained, the intensity of the peaks increases with temperature - the nanostructures become more crystalline. As represented in **Figure 3.15** the two peaks that correspond to the $Eu(OH)_3$ disappear at 300 °C and a new phase starts forming. There is a transformation of the $Eu(OH)_3$ to, probably, Eu_2O_3. The change from a hydroxide to an oxide is caused by thermal elimination of OH-groups [35].

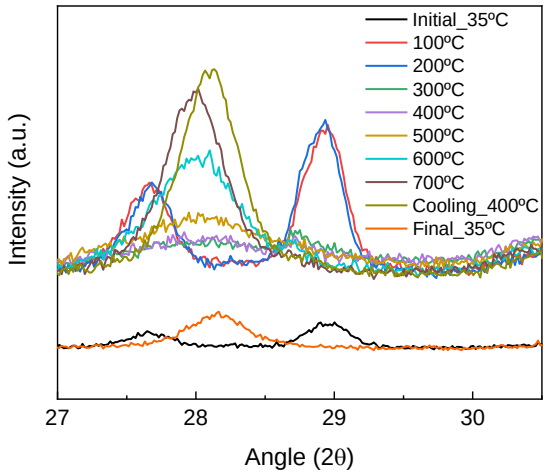

Figure 3.15 – XRD in-situ of ZnO MW NWs with 2% Eu dopant

To confirm that the nanostructures around the NWs correspond to $Eu(OH)_3$, Eu doped ZnO NWs dispersed on a Si substrate were annealed at 300 °C. On **Figure 3.16** is the before and after

annealing SEM images of NWs on the substrate. With only 300 °C of annealing there are less nanostructures around the NWs but the transformation appears to not be complete as there are still a few nanostructures present.

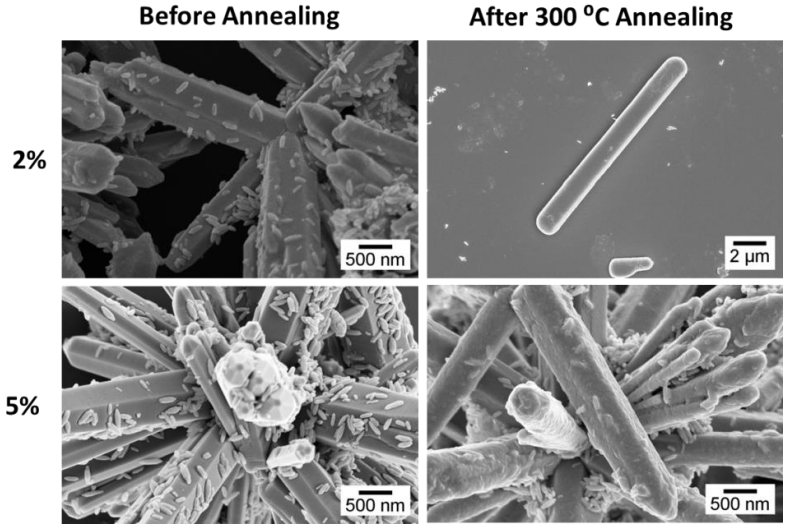

Figure 3.16 – Before and after 300 °C annealing of 2% and 5% Eu doped MW ZnO NW

In literature, the annealing temperature for europium is usually high (700 °C or more). [26] Armelao L. et al. actually suggest that a higher temperature allowed the removal of most -OH groups, but also promoted the crystallization of Eu_2O_3 (at 800 °C) [11].

XRD was again performed on the non-annealed sample and on the sample that suffered the 700 °C heating on the XRD in-situ process. The diffractograms can be seen in Appendix D. From the RT to the 700 °C, the peaks for the europium hydroxide are no longer visible and a new phase is formed that can be identified as europium oxide.

Optical characterization was performed on the doped NWs through UV-Nis spectroscopy and Raman. The bandgap was calculated and is summed up on **Table 3.5**, together with the calculated crystallite sizes.

Table 3.5 – Crystallite sizes and bandgap calculated for the Eu doped ZnO NWs

	CO		**MW**	
	Crystallite size [nm]	Eg [eV]	Crystallite size [nm]	Eg [eV]
Undoped	57.8	3.140	74.5	3.060
1%	79.9	-	94.5	3.198
2%	72.0	-	75.5	3.228
3%	93.4	-	83.2	3.234
4%	72.4	-	71.4	3.214
5%	102.2	-	100.7	3.237

As it can be seen, as the Eu content increases, the produced ZnO NWs become more crystalline for both synthesis routes. In fact the crystallite size increased from nearly 60 nm for the undoped NWs reaching near 100 nm for the doped ZnO with 5% Eu content in the CO route.

Comparing with the undoped, the bandgap showed an increase when the Eu was added to the synthesis but no clear tendency is found with the increasing dopant concentration.

Figure 3.17 shows the spectra of the undoped ZnO NWs and the europium doped ZnO NWs. The spectrum of the NWs that were annealed at 700 °C on the XRD chamber is also represented.

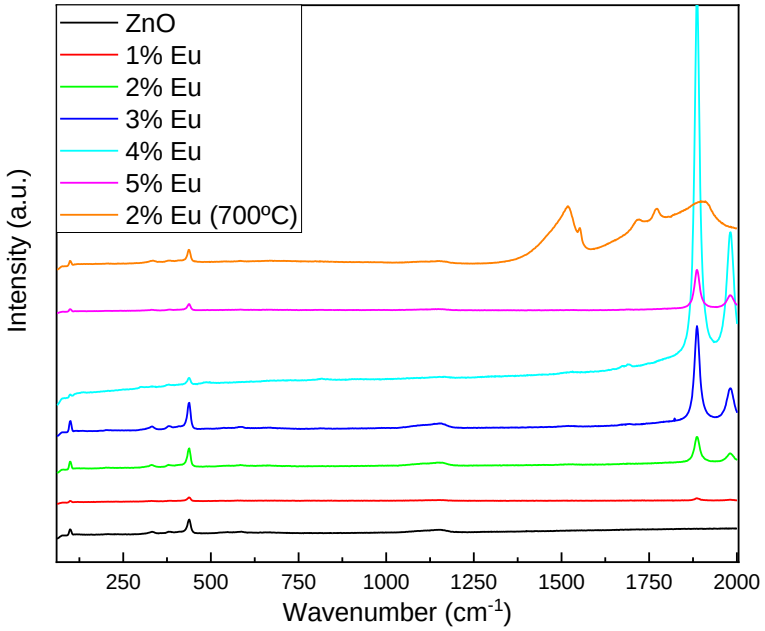

Figure 3.17 – Raman spectra of CO NWs doped with Eu

The peaks present in the graph can be identified with ZnO [47]. There are two peaks (1886 cm^{-1} and 1982 cm^{-1}) that in literature are associated with europium hydroxide [48]. The spectrum of the NWs that that were annealed at 700 °C still have the peaks correspondent to the bands of ZnO.

An attempt to align electric contacts on the Eu doped ZnO NWs was not attempted since the NWs produced are very aggregated. Optimizing the synthesis to obtain longer NWs with less agglomerates can permit the electrical characterization as done for the undoped ZnO NWs.

Chapter 4

4. Conclusions and Future Perspectives

For the undoped ZnO synthesis, it was possible to confirm the production of ZnO NWs with hexagonal wurtzite ZnO crystalline structure for both synthesis routes. The MW route produced nanoflowers while the CO route leads to less agglomerates.

It was possible to test the UV response of the produced NWs with the use of interdigital contacts. Even if the produced devices are not reproducible, it can be said that UV sensors were successfully achieved.

The alignment of contacts on individual NWs was improved, there is an increased yield since the previous work. Two methods were evaluated for the alignment of contacts on isolated NWs. Comparing method A with method B, method B seems to be more stable, as the number of working devices obtained is higher. The passivation layer may help with the adhesion of the NWs to the substrate. Regarding the UV irradiation, the devices from method A have a superior increase on the output current; the parylene layer conditionates the sensing mechanism of the ZnO to the UV light.

AFM-SKPFM showed to be a promising technique to calculate the work function of the NWs.

With the Eu doped ZnO synthesis it was also possible to confirm the hexagonal wurtzite ZnO crystalline structure. The produced NWs (without any thermal treatment) have europium hydroxide nanostructures attached to the surface. After a thermal treatment (annealing > 300 °C) this phase disappears and a new one is formed – europium oxide. It is still not confirmed that the ZnO is being doped and that the Eu is entering the ZnO crystalline network.

As for the future, an enhanced statistical analysis is required to better assess the reliability and repeatability of the methods. With that said, the alignment methodology can still be optimized in order to have a higher number of working devices. A more uniform method to place the NWs upon the interdigital contacts should be pursued. This is a simpler technique that permits the characterization of the NWs but a more uniform method is needed. For instance, the use of a binder with the nanopowder could form a more uniform distribution of the nanostructures in a film.

For the Eu doped the post annealing treatment should be studied to comprehend better the doping process. XPS can be used to really understand if the ZnO nanostructure lattice is being doped with Eu ions.

5. Bibliography

[1] D. Nunes *et al.*, *Metal Oxide Nanostructures: Synthesis, Properties and Applications*. Elsevier Science, 2018.

[2] V. V. Pokropivny and V. V. Skorokhod, "Classification of nanostructures by dimensionality and concept of surface forms engineering in nanomaterial science," *Mater. Sci. Eng. C*, vol. 27, no. 5–8 SPEC. ISS., pp. 990–993, 2007.

[3] J. N. Tiwari, R. N. Tiwari, and K. S. Kim, "Zero-dimensional, one-dimensional, two-dimensional and three-dimensional nanostructured materials for advanced electrochemical energy devices," *Prog. Mater. Sci.*, vol. 57, no. 4, pp. 724–803, 2012.

[4] N. P. Dasgupta, J. Sun, C. Liu, S. Brittman, and S. C. Andrews, "25th Anniversary Article : Semiconductor Nanowires – Synthesis , Characterization , and Applications," pp. 2137–2184, 2014.

[5] S. Walia *et al.*, "Transition metal oxides - Thermoelectric properties," *Prog. Mater. Sci.*, vol. 58, no. 8, pp. 1443–1489, 2013.

[6] Z. L. Wang, "Zinc oxide nanostructures : growth , properties and applications applications," *J. Phys.*, 2004.

[7] A. Pimentel, S. H. Ferreira, D. Nunes, T. Calmeiro, R. Martins, and E. Fortunato, "Microwave synthesized ZnO nanorod arrays for UV sensors: A seed layer annealing temperature study," *Materials (Basel).*, vol. 9, no. 4, 2016.

[8] R. Hong, T. Pan, J. Qian, and H. Li, "Synthesis and surface modification of ZnO nanoparticles," *Chem. Eng. J.*, 2006.

[9] A. S. Lanje, S. J. Sharma, R. S. Ningthoujam, J. S. Ahn, and R. B. Pode, "Low temperature dielectric studies of zinc oxide (ZnO) nanoparticles prepared by precipitation method," *Adv. Powder Technol.*, 2013.

[10] S. A. Vorobyova, A. I. Lesnikovich, and V. V. Mushinskii, "Interphase synthesis and characterization of zinc oxide," *Mater. Lett.*, 2004.

[11] L. Armelao *et al.*, "Structure-luminescence correlations in europium-doped sol-gel Zno nanopowders," *J. Phys. Chem. C*, vol. 112, no. 11, pp. 4049–4054, 2008.

[12] K. L. Foo, U. Hashim, K. Muhammad, and C. H. Voon, "Sol–gel synthesized zinc oxide nanorods and their structural and optical investigation for optoelectronic application," *Nanoscale Res. Lett.*, vol. 9, no. 1, pp. 1–10, 2014.

[13] Q. Li, C. Wang, M. Ju, W. Chen, and E. Wang, "Polyoxometalate-assisted electrochemical deposition of hollow ZnO nanospheres and their photocatalytic properties," *Microporous*

Mesoporous Mater., 2011.

[14] A. Kolodziejczak-Radzimska and T. Jesionowski, "Zinc oxide-from synthesis to application: A review," *Materials (Basel).*, vol. 7, no. 4, pp. 2833–2881, 2014.

[15] "Microwave synthesis: chemistry at the speed of light," *Choice Rev. Online*, 2003.

[16] R. M. and E. F. Ana Pimentel, Daniela Nunes, Sónia Pereira, "Photocatalytic Activity of TiO2 Nanostructured Arrays Prepared by Microwave-Assisted Solvothermal Method," *Intech open*, vol. 2, p. 64, 2012.

[17] E. T. Thostenson and T. W. Chou, "Microwave processing: fundamentals and applications," *Compos. Part A Appl. Sci. Manuf.*, 1999.

[18] S. Materials, "Metal Oxide Nanostructures for Sensor Applications," pp. 0–22, 2019.

[19] A. Samouco, A. C. Marques, A. Pimentel, R. Martins, and E. Fortunato, "Laser-induced electrodes towards low-cost flexible UV ZnO sensors," *Flex. Print. Electron.*, vol. 3, no. 4, pp. 0–21, 2018.

[20] F. Wall, "Rare earth elements," 2014.

[21] S. Geburt *et al.*, "Rare Earth Doped Zinc Oxide Nanowires," vol. 8, no. 1, 2008.

[22] S. A. Al Rifai and B. A. Kulnitskiy, "Microstructural and optical properties of europium-doped zinc oxide nanowires," *J. Phys. Chem. Solids*, vol. 74, no. 12, pp. 1733–1738, 2013.

[23] D. Wang, G. Xing, M. Gao, L. Yang, J. Yang, and T. Wu, "Defects-mediated energy transfer in red-light-emitting Eu-doped ZnO nanowire arrays," *J. Phys. Chem. C*, vol. 115, no. 46, pp. 22729–22735, 2011.

[24] X. Zeng, J. Yuan, and L. Zhang, "Synthesis and photoluminescent properties of rare earth doped ZnO hierarchical microspheres," *J. Phys. Chem. C*, vol. 112, no. 10, pp. 3503–3508, 2008.

[25] P. Kumar and Y. K. Walia, "Synthesis and Structural properties of Zinc Oxide Nano Particles (ZnO NPs): A Review," *Asian J. Adv. Basic Sci.*, vol. 2, no. 3, pp. 39–49, 2014.

[26] A. Pimentel *et al.*, "Synthesis of Long ZnO Nanorods under Microwave Irradiation or Conventional Heating," 2014.

[27] Y. Zhang, M. K. Ram, E. K. Stefanakos, and D. Y. Goswami, "Synthesis, characterization, and applications of ZnO nanowires," *J. Nanomater.*, vol. 2012, 2012.

[28] L. Li *et al.*, "Hydrothermal synthesis and gas sensing properties of single-crystalline ultralong ZnO nanowires," *Appl. Phys. A Mater. Sci. Process.*, 2010.

[29] J. Goldberger, D. J. Sirbuly, M. Law, and P. Yang, "ZnO nanowire transistors," *J. Phys. Chem. B*, vol. 109, no. 1, pp. 9–14, 2005.

[30] Y. F. Lin, W. B. Jian, Z. Y. Wu, F. R. Chen, J. J. Kai, and J. J. Lin, "Determination of contact and intrinsic nanowire resistivity in two-contact ZnO nanowire devices," *2008 2nd IEEE Int. Nanoelectron. Conf. INEC 2008*, pp. 1112–1115, 2008.

[31] D. Coelho, "Solution Based Synthesis of ZnO Nanorods for Optoelectronic Applications," Faculty of Sciences and Technology, NOVA University of Lisbon, 2019.

[32] B. D. Cullity and S. R. Stock, "Elements of X-ray diffraction, 3rd edition," *Prentice Hall*, 2001.

[33] A. Pimentel *et al.*, "Effect of solvents on ZnO nanostructures synthesized by solvothermal method assisted by microwave radiation: a photocatalytic study," *J. Mater. Sci.*, vol. 50, no. 17, pp. 5777–5787, Sep. 2015.

[34] Y. Il Jung, S. H. Baek, and I. K. Park, "Growth of Eu-doped ZnO nanorods on silicon substrate by low temperature hydrothermal method," *Thin Solid Films*, vol. 546, pp. 259–262, 2013.

[35] E. Wolska-Kornio, J. Kaszewski, B. S. Witkowski, Wachnicki, and M. Godlewski, "The effect of annealing on properties of europium doped ZnO nanopowders obtained by a microwave hydrothermal method," *Opt. Mater. (Amst).*, vol. 59, pp. 103–106, 2016.

[36] J. Tauc, "Optical properties and electronic structure of amorphous Ge and Si," *Mater. Res. Bull.*, vol. 3, no. 1, pp. 37–46, Jan. 1968.

[37] Z. Zhang *et al.*, "Growth and Electrical Properties of Zinc Oxide Nanowires," *J. Nanosci. Nanotechnol.*, vol. 9, pp. 1119–1122, 2009.

[38] V. Srikant and D. R. Clarke, "On the optical band gap of zinc oxide," *J. Appl. Phys.*, 1998.

[39] M. H. Mamat, Z. Khusaimi, M. M. Zahidi, and M. R. Mahmood, "Performance of an ultraviolet photoconductive sensor using well-aligned aluminium-doped zinc-oxide nanorod arrays annealed in an air and oxygen environment," *Jpn. J. Appl. Phys.*, 2011.

[40] C. Y. Chen, P. H. Chang, K. T. Tsai, and J. H. He, "Electrical and optoelectronic characterization of a ZnO nanowire contacted by focused-ion-beam-deposited Pt," in *INEC 2010 - 2010 3rd International Nanoelectronics Conference, Proceedings*, 2010.

[41] C. H. Liu, W. C. Yiu, F. C. K. Au, J. X. Ding, C. S. Lee, and S. T. Lee, "Electrical properties of zinc oxide nanowires and intramolecular p-n junctions," *Appl. Phys. Lett.*, 2003.

[42] Z. Fan, D. Wang, P. C. Chang, W. Y. Tseng, and J. G. Lu, "ZnO nanowire field-effect transistor and oxygen sensing property," *Appl. Phys. Lett.*, vol. 85, no. 24, pp. 5923–5925, 2004.

[43] H. Seo, D. Goo, and G. Jung, "How to obtain sample potential data for KPFM measurement," *Park Syst. | Enabling Nanoscale Adv.*, vol. Applicatio, p. 4.

[44] C. J. Lee, T. J. Lee, S. C. Lyu, Y. Zhang, H. Ruh, and H. J. Lee, "Field emission from well-aligned zinc oxide nanowires grown at low temperature," *Appl. Phys. Lett.*, vol. 81, no. 19, pp. 3648–3650, 2002.

[45] X. Bai, E. G. Wang, P. Gao, and Z. L. Wang, "Measuring the work function at a nanobelt tip

and at a nanoparticle surface," *Nano Lett.*, vol. 3, no. 8, pp. 1147–1150, 2003.

[46] Y. Chen *et al.*, "In Situ Characterization of the Local Work Function along Individual Free Standing Nanowire by Electrostatic Deflection," *Sci. Rep.*, vol. 6, no. January, pp. 1–7, 2016.

[47] R. Zhang, P. G. Yin, N. Wang, and L. Guo, "Photoluminescence and Raman scattering of ZnO nanorods," *Solid State Sci.*, vol. 11, no. 4, pp. 865–869, 2009.

[48] S. Fang, J. Tang, L. Gao, and L. Zhou, "Preparation and characterization of multiwalled carbon nanotubes deposited by europium hydroxide," *Adv. Mater. Res.*, vol. 418–420, pp. 428–435, 2012.

Appendices

Appendix A – UV sensors

Optical microscope images for the three different UV sensors tested where it is clear the non-uniform distribution of nanostructures.

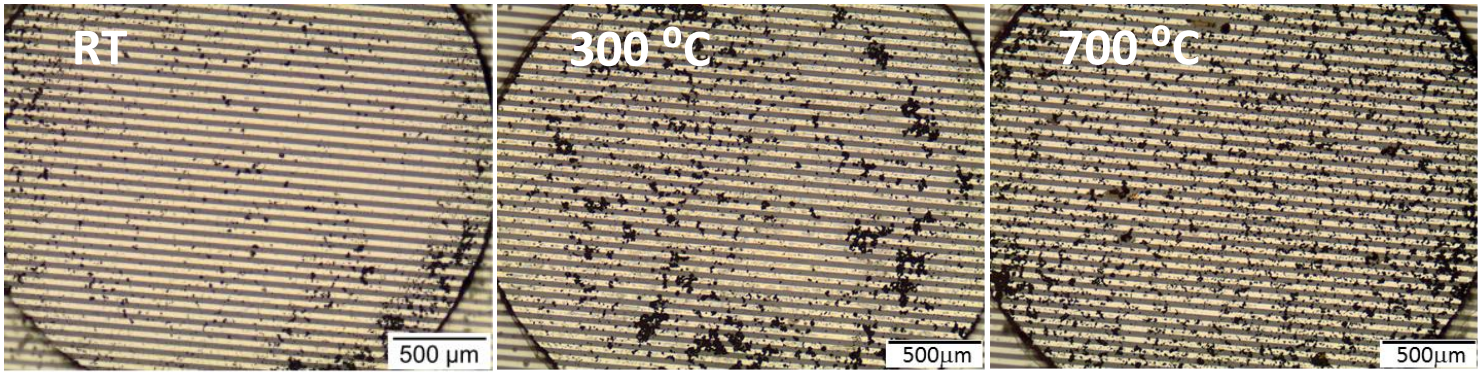

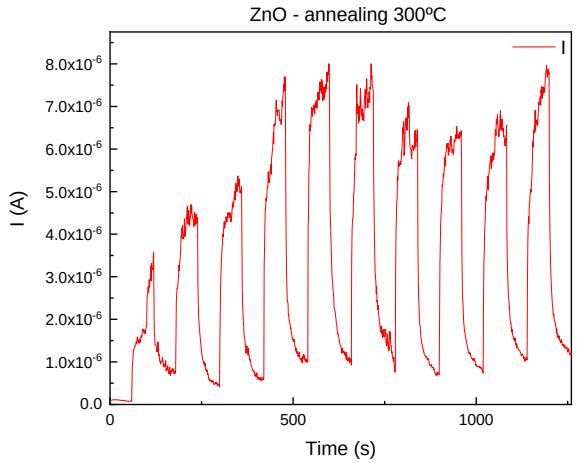

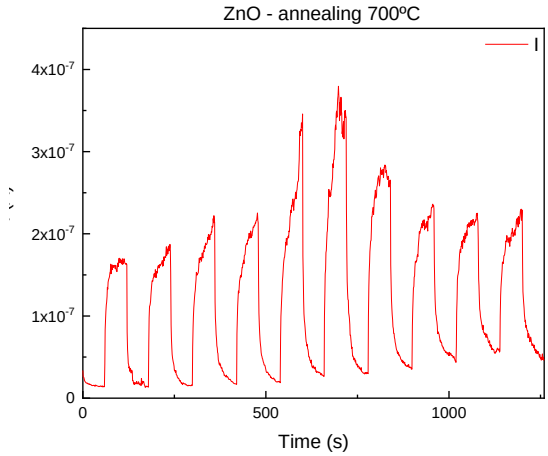

Appendix B – Tauc Plots (band gap calculation)

From the Spectrometer UV-Vis-NIR it is obtained a graph of %R in function of the electromagnetic radiation wavelength.

Plotting a graph using the Tauc relation it is possible to extract the Eg value [7][36]

$$(\alpha h\nu)^m = A(h\nu - E_g)$$

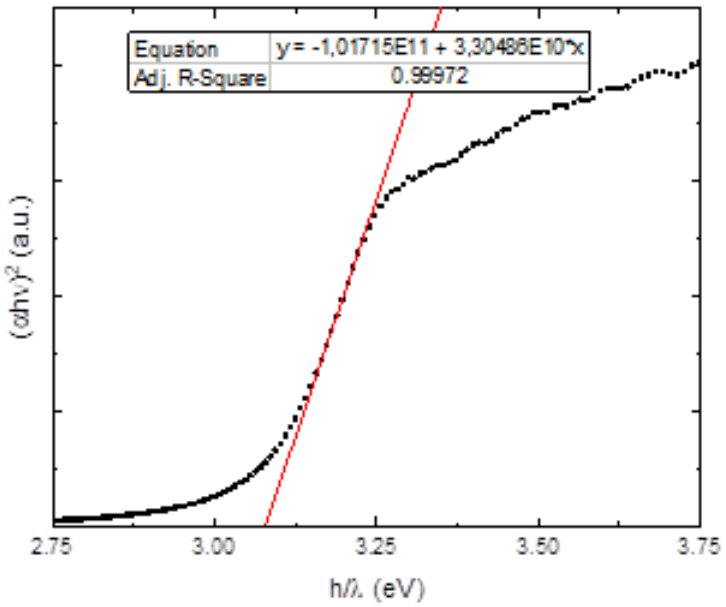

Where Eg is the material optical band gap, h is the Plank constant (H = 4.135×10^{-5} eV s), v is the frequency, α is the material absorption coefficient, m is the constant that depends on the type of optical transition (m = 2 for allowed indirect transitions and m = 1/2 for allowed direct transition) and A is an energy-independent constant.

The intersection of the linear fit with the X axis corresponds to the band gap of the sample.

Appendix C – Individual NW characterization

All data for each working individual NW is presented.

I_D is the current measured in the NW and I_G is the leakage current

Method A

600 °C

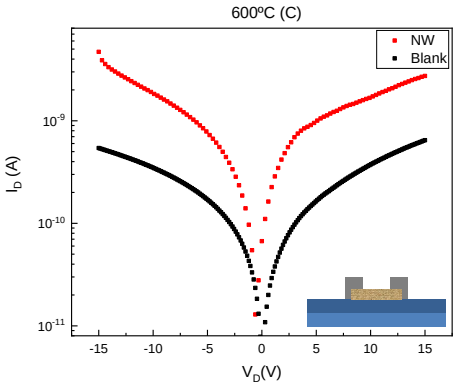

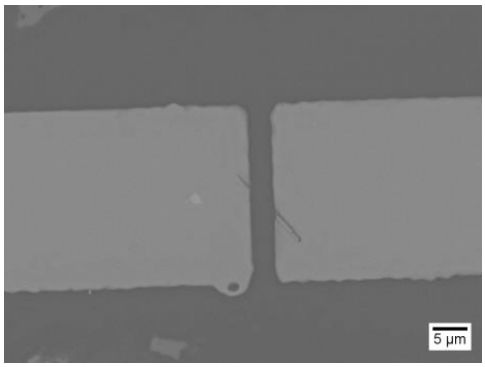

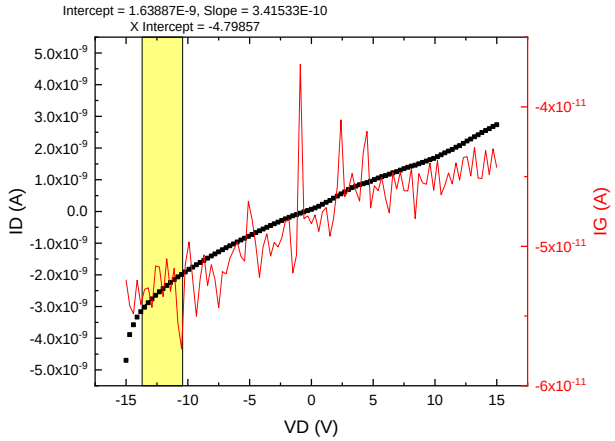

Method A

700 °C

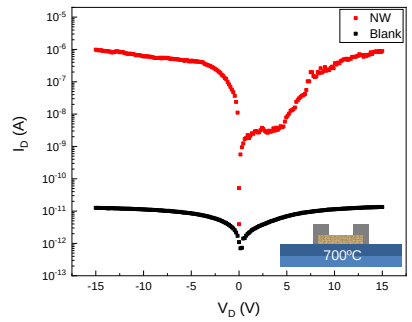

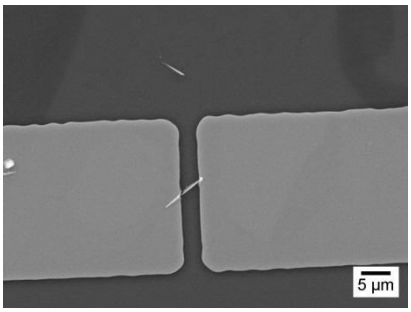

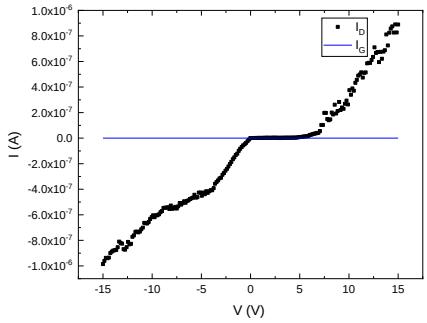

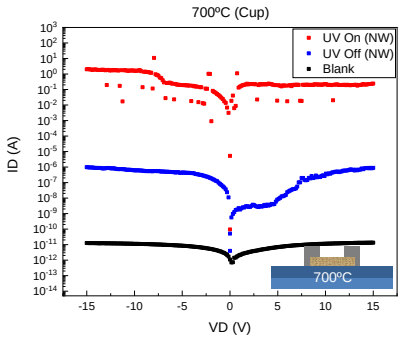

Method B

RT (B) *

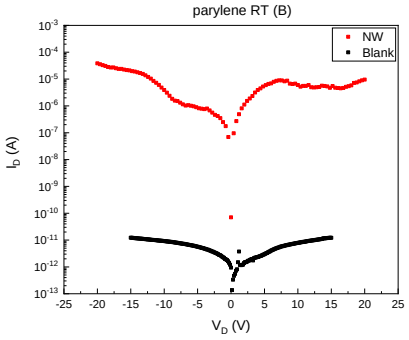
parylene RT (B)
NW
Blank
I_D (A)
V_D (V)

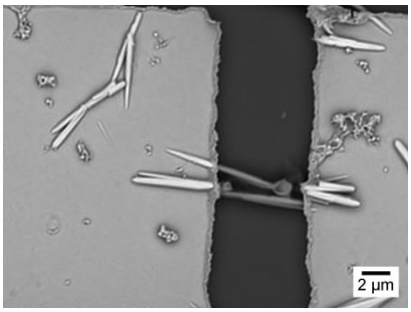
2 µm

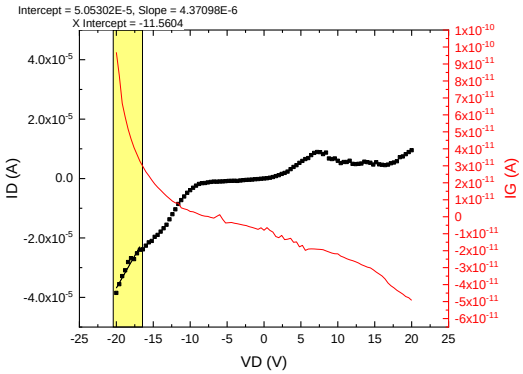
Intercept = 5.05302E-5, Slope = 4.37098E-6
X Intercept = -11.5604
ID (A)
IG (A)
VD (V)

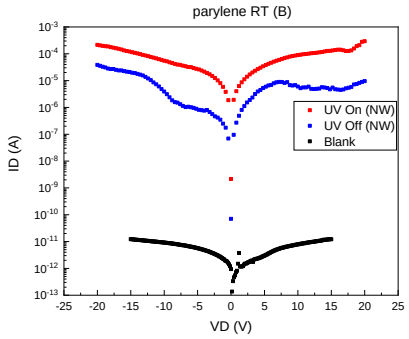
parylene RT (B)
UV On (NW)
UV Off (NW)
Blank
ID (A)
VD (V)

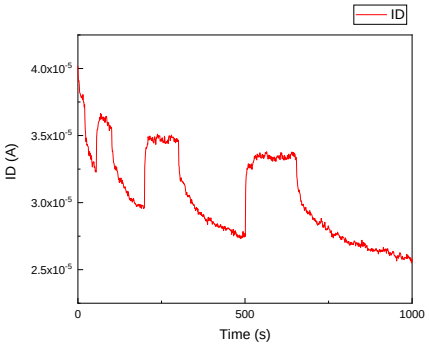
ID
ID (A)
Time (s)

Method B

RT (D) *

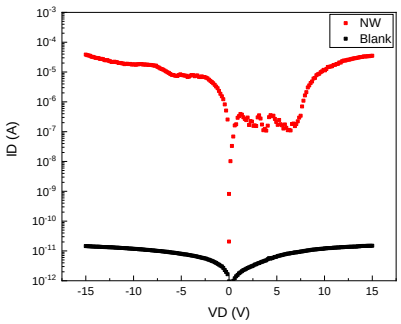
NW
Blank
ID (A)
VD (V)

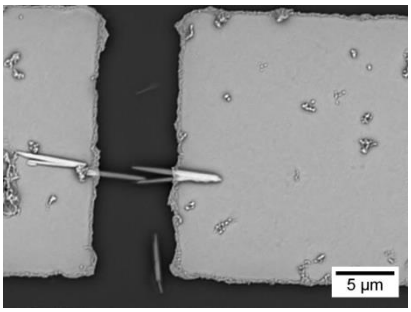
5 µm

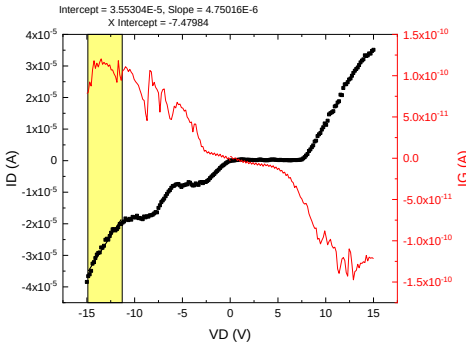
Intercept = 3.55304E-5, Slope = 4.75016E-6
X Intercept = -7.47984
ID (A)
VD (V)

Method B

RT (E) *

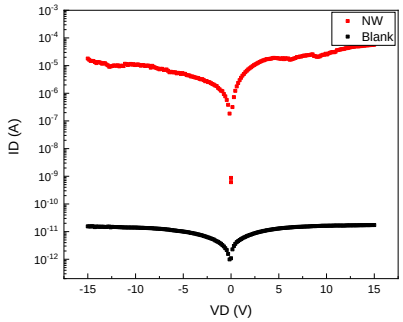
NW
Blank
ID (A)
VD (V)

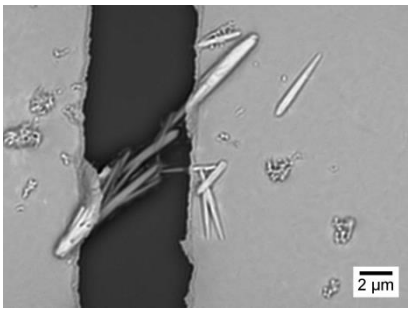
2 µm

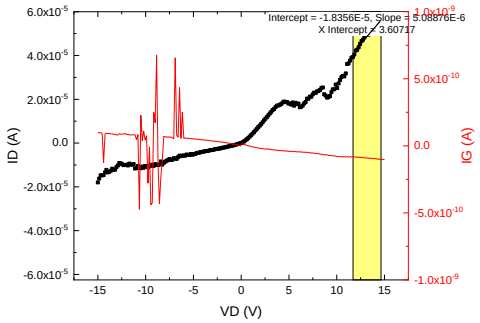
Intercept = -1.8356E-5, Slope = 5.08876E-6
X Intercept = 3.60717
ID (A)
IG (A)
VD (V)

Method B

300 °C (C)

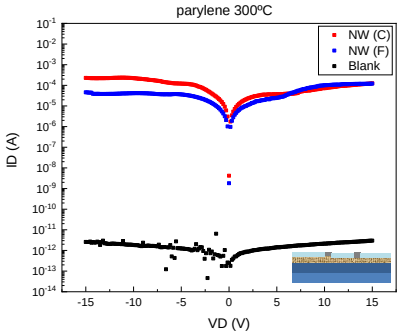

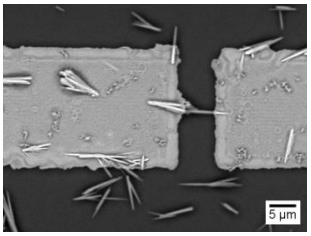

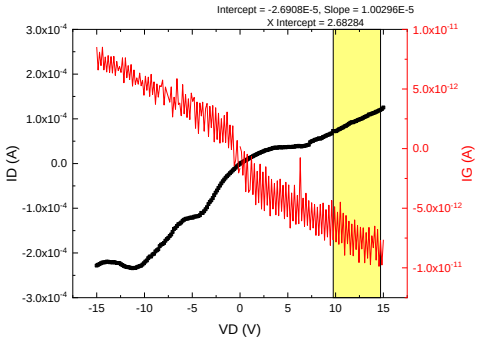

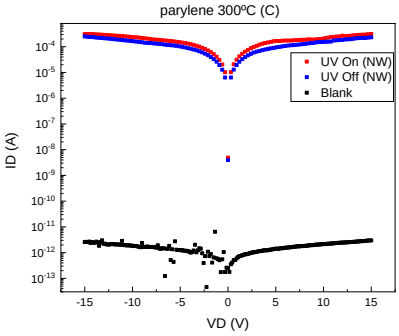

Method B

300 °C (F)

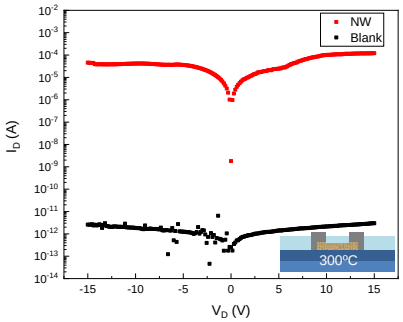

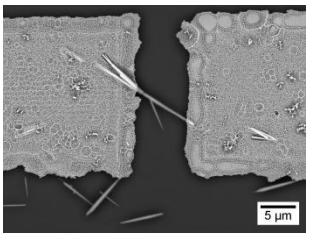

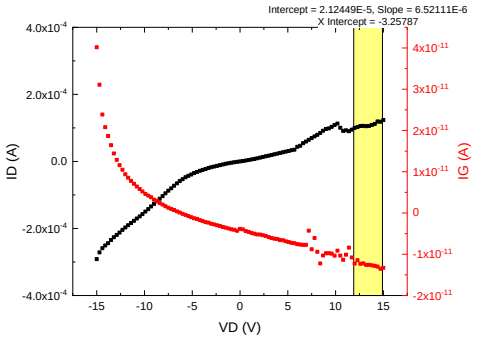

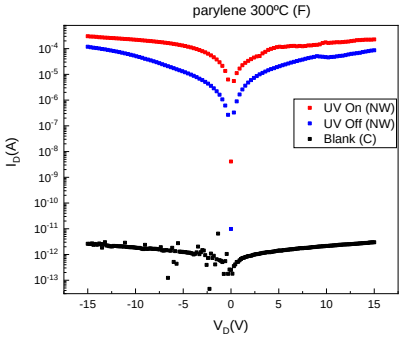

Method B

700 °C (B)

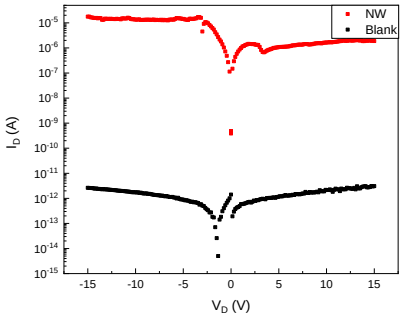

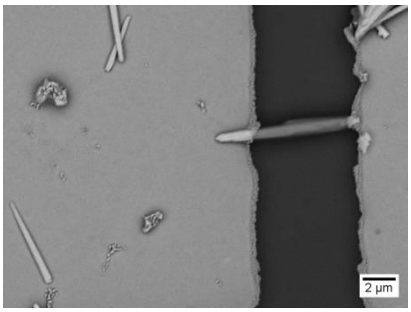

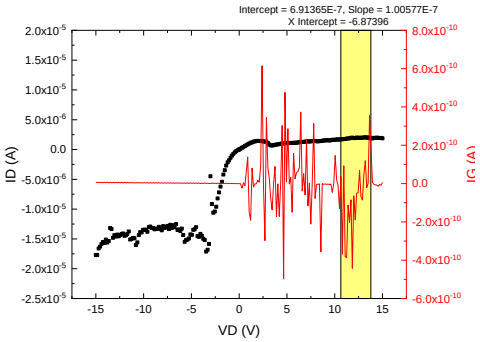

Method B

700 °C (E) *

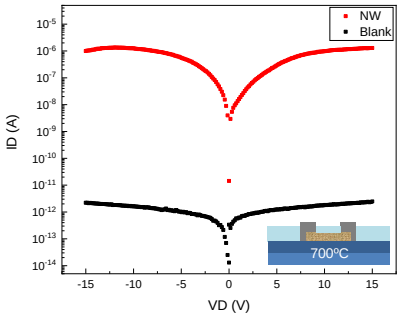

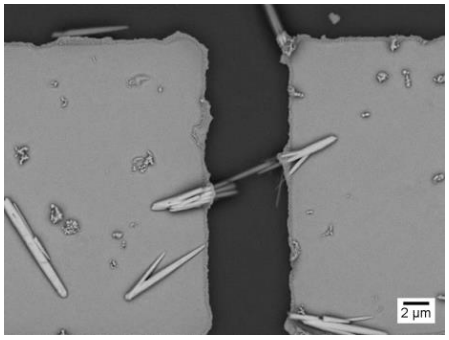

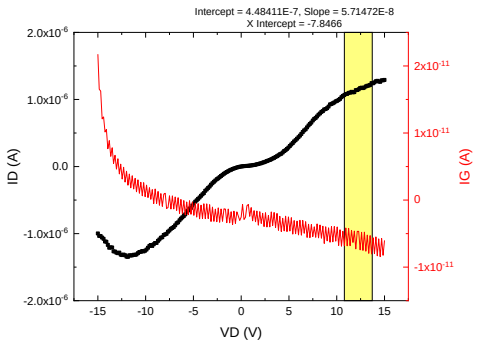

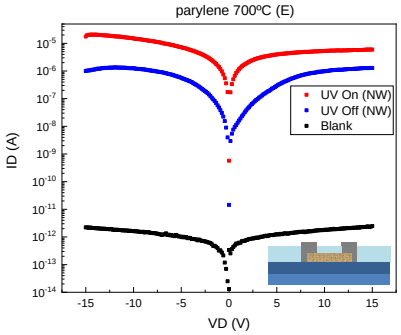

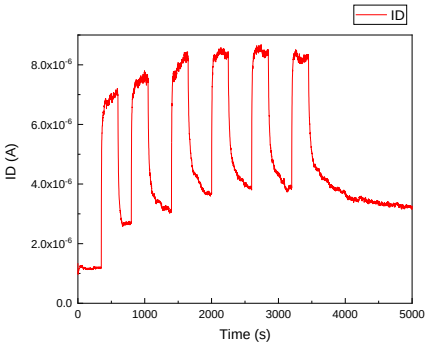

Appendix D

Comparison between XRD diffractograms for the 2% Eu doped ZnO NWs without annealing and with a 700 ºC annealing (performed on the XRD chamber in an in-situ measurement).

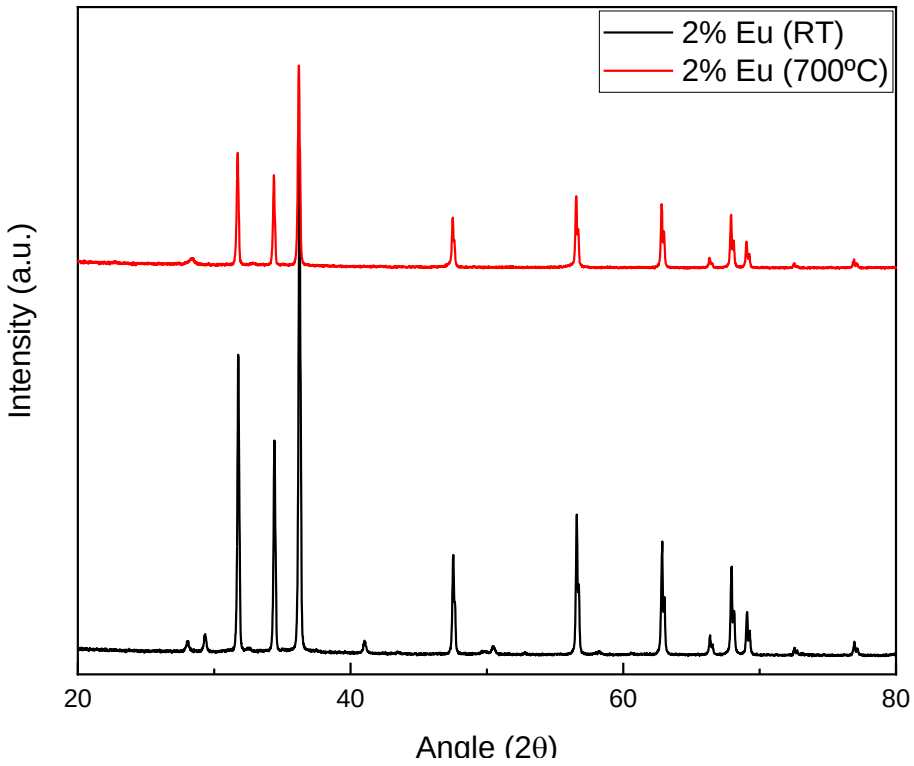

Figure 6.1 – XRD of ZnO NWs doped with 2% Eu before and after annealing at 700 °C